Environmental Microbiome

RESEARCH

Open Access

Metabolic redundancy and specialisation of novel sulfide-oxidizing *Sulfurimonas* and *Sulfurovum* along the brine-seawater interface of the Kebrit Deep

Rayyan Alamoudi[1†], Alan Barozzi[1†], Grégoire Michoud[1], Marc W. Van Goethem[1], Charlene Odobel[1], Yue Chen[1], Ramona Marasco[1*] and Daniele Daffonchio[1,2*]

Abstract

Background Members of the Campylobacterota phylum are dominant key players in sulfidic environments, where they make up a stable portion of sulfide-oxidizing bacterial communities. Despite the significance of these bacteria in primary production being well recognised in several ecosystems, their genomic and metabolic traits in sulfidic deep hypersaline anoxic basins (DHABs) remain largely unexplored. This knowledge gap not only hampers our understanding of their adaptation and functional role in DHABs but also their ecological interactions with other microorganisms in these unique ecosystems.

Results Metabolic reconstructions from metagenome-assembled genomes (MAGs) of sulfide-oxidizing Campylobacterota were conducted at 10 cm spatial resolution within the halocline of the brine-seawater interface (BSI, salinity 91–155 PSU) of the 1466 m deep sulfidic Kebrit Deep in the Red Sea. Fifty-four Campylobacterota MAGs were assembled and dereplicated into three distinct groups, with the highest-quality genome retained as representative. These genomes represent novel sulfide-oxidizing species within the *Sulfurimonas* and *Sulfurovum* genera, which differ from those found in mildly saline deep-sea sulfidic pools. They are stratified along the BSI and utilise the reductive tricarboxylic acid cycle to fix carbon dioxide, acting as primary producers. Their energy generation processes include aerobic or anaerobic-nitrate-dependent sulfide oxidation, as well as hydrogen oxidation. In addition to the osmoprotectant pathways commonly observed in Campylobacterota, such as the synthesis and uptake of proline and glutamate, the two Kebrit Deep *Sulfurovum* species exhibit genomic signatures for ectoine synthesis, further aiding their adaptation to high salinity. This combination of metabolic redundancy and specialisation within the confined spatial boundaries (~1 m) of the BSI is pivotal in governing microbial interactions, including those with sulfate-reducers, heterotrophs, and other primary producers.

Conclusions These results show how the selective pressures mediated by the sulfidic and hypersaline conditions of Kebrit Deep have resulted in novel, adapted and metabolically redundant *Sulfurimonas* and *Sulfurovum* species

[†]Rayyan Alamoudi and Alan Barozzi have contributed equally to this work.

*Correspondence:
Ramona Marasco
ramona.marasco@kaust.edu.sa
Daniele Daffonchio
daniele.daffonchio@kaust.edu.sa
Full list of author information is available at the end of the article

that contribute to the energy coupling, nutrient turnover and metabolic continuity along the physico-chemical gradient of the BSI.

Keywords Deep hypersaline anoxic basin (DHAB), Sulfidic DHAB, Brine pool, Sulfur metabolism, Campylobacterota, Metabolic adaptation, Microbial networking, Metagenome, Red Sea

Background

Bacteria affiliated with the Campylobacterota phylum (formerly *Epsilonproteobacteria* class) are key players in the sulfur cycle on a global scale [1–5]. Sulfur compounds are ubiquitous in marine ecosystems. For instance, in the seawater column, besides the oxidised sulfate, reduced forms are enriched in oxygen-minimum zones [6–8]. Sulfur species concentrations may be particularly high in other environments, such as sulfide-rich deep-sea hydrothermal vents and cold seeps, as well as deep hypersaline anoxic basins (DHABs) where highly concentrated brines persist at the seabed [1, 2, 9–13]. In these environments, reduced sulfur compounds like hydrogen sulfide, elemental sulfur, and thiosulfate serve as energy sources for the chemolithoautotrophic metabolism of sulfide/sulfur-oxidizing microorganisms, among which Campylobacterota are highly represented [14–16].

The metabolic capabilities of sulfide/sulfur-oxidizing Campylobacterota have been extensively examined in hydrothermal vents and cold seeps by characterising novel isolates [17–19] and genomes reconstructed from metagenomes [20]. These studies revealed versatile metabolisms, wherein sulfur compounds (such as sulfide/sulfur/thiosulfate) act as electron donors and are coupled with various oxidised species as electron acceptors, including oxygen, nitrogen, manganese, and iron [14, 21–24]. This coupling generates the electron flow and reducing-power that fuels autotrophic dark carbon fixation in Campylobacterota, performed via the reverse tricarboxylic acid (rTCA) cycle [25, 26]. However, horizontal gene transfer events can result in the acquisition of alternative ways to fix carbon, as observed in the epibiont *Candidatus* Thiobarba in which rTCA was substituted by the Calvin–Benson–Bassham (CBB) cycle [27]. Among frequently encountered Campylobacterota, *Sulfurimonas* can utilise reduced sulfur compounds and hydrogen as electron donors, aerobically with oxygen or anaerobically with nitrate or nitrite as electron acceptors [28]. Another genus with similar metabolic capabilities, *Sulfurovum*, has been shown to inhabit the Urania DHAB in the Mediterranean Sea [1]. Within Campylobacterota (referred to as ε-proteobacteria), the relative abundance of such *Sulfurovum* increased along the salinity gradient, reaching up to 70% of the relative abundance at a salinity of 181 PSU [1]. Sulfur-oxidizing bacteria typically gain energy through the thiosulfate oxidation pathway genes (SOX), even if incomplete forms of this pathway have been identified in several cases [29]. These bacteria may also utilise alternative sulfur oxidation mechanisms, such as those involving sulfide:quinone oxidoreductase (SQR), demonstrating metabolic versatility in adapting to varying environmental sulfur conditions [30]. The literature on Campylobacterota accurately positions these sulfide/sulfur oxidisers as dominant pioneer colonisers of sulfidic (extreme) environments, supporting metabolic networks and microbial succession patterns [31].

The genetic metabolic potential and genotypic variation (i.e., redundancy and specialisation) of *Sulfurimonas* and *Sulfurovum* remain elusive in DHABs, even if they have been identified as relevant players in terms of number and diversity in such ecosystems [1, 26, 32]. Yet, so far, no sulfide/sulfur-oxidizing Campylobacterota have been obtained in culture or their genome reconstructed from metagenomes from highly saline DHABs. The *Sulfurimonas* and *Sulfurovum*—whose genomes were recently assembled from small (few meters wide) deep-sea pools (ca. 1150 m depth) in the south-eastern Mediterranean Sea—live at a salinity slightly higher than that of seawater (range of 40–60 PSU) [33]. This is much lower than the salinity of the Mediterranean or Red Sea DHABs, which reach values far above 200 PSU in the brine body [3].

In this work, we aim to contribute to filling this knowledge gap by understanding the diversity and metabolic potential of Campylobacterota inhabiting the most densely populated portion of DHABs [10, 34], the brine-seawater interface (BSI, salinity range 91–155 PSU) of the sulfidic Kebrit Deep DHAB in the Red Sea. The name "Kebrit" originates from Arabic and signifies sulfur, underscoring its status as one of the most sulfidic DHABs among those known in the Red Sea [35, 36]. Its salinity increases from ca. 40 PSU in the deep Red Sea waters to 218 PSU in the brine body [37–39]. In DHABs, the BSI encloses a vertical succession of electron donors/acceptors coupled in a narrow space that ranges from one to a few meters. Such a gradient allows the flourishing of taxonomically unrelated bacteria that can exploit different redox couples for their metabolisms [1, 3, 10, 32]. We hypothesise that Campylobacterota inhabiting the sulfidic, hypersaline, and geographically isolated Kebrit Deep may undergo unique evolutionary trajectories and selection processes compared to their counterparts in other deep-sea habitats. The combination of

geographical isolation and the selective pressure imposed by the extreme environmental conditions of DHABs could indeed drive the development of distinct metabolic adaptations and specialisation traits, enhancing the metabolic versatility of Campylobacterota.

Using a previously established precise sampling strategy [1, 3, 10, 40], we collected water fractions corresponding to about 10 cm-thick layers along the Kebrit Deep BSI (Additional file Fig. S1) and obtained independent metagenomes for each layer. We were able to identify three novel sulfide-oxidizing Campylobacterota within the *Sulfurimonas* and *Sulfurovum* genera, define their stratification along the BSI, reconstruct their metabolisms from the metagenome-assembled genomes (MAGs) and establish their networking properties with the other bacteria thriving along the BSI of Kebrit Deep. The novel Campylobacterota have been proposed as three novel *Candidatus* species in accordance with the International Code of Nomenclature of Prokaryotes (ICNP) guidelines for uncultivated microbial species, with the proposed names *Candidatus* Sulfurimonas kebritiensis, *Candidatus* Sulfurovum kebritense, and *Candidatus* Sulfurovum profundilacunae, respectively.

Materials and methods

Sampling of the Kebrit Deep BSI The BSI of Kebrit Deep (24°44.000′N, 36°17.000′E; Fig. 1A) was sampled during an expedition conducted in July 2016 with the Coastal and Marine Resources Core Lab (CMOR, KAUST) R/V Thuwal, using a Rosette system equipped with 23 Niskin bottles (Additional file Fig. S1) and an Idronaut Conductivity, Temperature, and Depth (CTD) sensor system equipped with an oxygen probe to measure the salinity, temperature, oxygen and depth profiles, as described in previous studies [10, 40]. Briefly, the Rosette sampler was dispatched above Kebrit Deep until an increase in salinity was detected, marking the beginning of the BSI (Additional file Fig. S2). Once the BSI was reached, the Niskin bottles were closed sequentially following the salinity increase to entrap the BSI gradient. Immediately upon retrieving the Rosette on board, each Niskin bottle was checked by measuring the salinity at the top and the bottom with a manual refractometer (VWR) (Additional file Fig. S1). The Niskin bottle displaying the widest salinity gradient was sub-sampled into 1 L fractions (corresponding to ~10 cm layer of the BSI), resulting in nine samples covering the entire salinity gradient (Fig. 1B, C, Additional file Figs. S1 and S2). Samples of seawater and brine body from the two extremes of BSI were also collected with separate Niskin bottles (Fig. 1B); two from the seawater and one from the brine body. For each sample, salinity and pH were further measured using a 556 YSI Multiparameter detector before the water was filtered by a vacuum pump and percolator filtering system through a 0.2 µm polyethersulfone (PES) membrane. In total, we obtained 12 filters: two from seawater, nine from BSI layers and one from brine body. Each filter was then stored in lysis buffer (EDTA 40 mM pH 8.0, Tris–HCl 50 mM

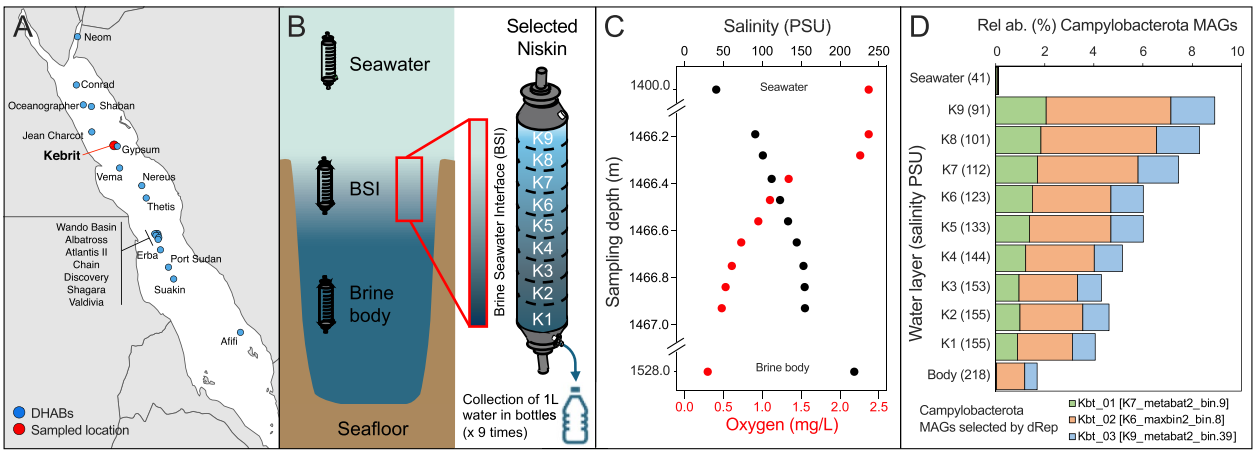

Fig. 1 Chemocline of Kebrit Deep BSI and associated Campylobacterota diversity. **A** Map of the Red Sea indicating the location of known DHABs (blue circles) and the sampled Kebrit Deep (red circle). **B** Schematic representation of Kebrit Deep DHAB, including seawater, brine-seawater interface (BSI) and brine body. Niskin bottles are reported to indicate the samples collected in these three portions. While water enclosed in the Niskin bottles from seawater and brine body are used to collect the samples as they are, the selected Niskin bottle enclosing the BSI gradient (see Additional file Figs. S1 and S2) is used to obtain 10 cm water layers (~1 L) in sterile bottles for a total of nine fractions (K1-K9). **C** CTD profiles of salinity (PSU) and oxygen (mg/L) at different depths measured during the sampling cast. **D** The relative abundance of the three MAGs identified as *Sulfurimonas* (Kbt_01) and *Sulfurovum* (Kbt_02 and Kbt_03) was computed by mapping the metagenomic sequences back to the MAGs using BBMap. Relative abundance (x-axis) is reported as a percentage (%) for each sample (y-axis), encompassing one seawater (41 PSU), nine BSI layers (K1-K9, 91–155 PSU) and one brine body (218 PSU). Taxonomy was reported following NCBI nomenclature

pH 8.0, sucrose 0.75 M) and flash-frozen in liquid nitrogen before being transferred to −80 °C until the DNA extraction was performed.

DNA extraction The total DNA from each filter was extracted using a phenol:chloroform:isoamyl alcohol (25:24:1, v/v) extraction protocol [40]. Briefly, the filters preserved in lysis buffer were incubated at 37 °C for 30 min with 20 mg/mL of lysozyme to lyse cells (Sigma-Aldrich). Then, 20 mg/mL proteinase K (Invitrogen) and 1% final concentration SDS were added and incubated for two hours at 55 °C. Next, the supernatant was carefully transferred into a fresh 15 mL falcon tube, and 1 volume of phenol:chloroform:isoamyl alcohol (25:24:1, pH 7.7–8.3) was added. The contents of the falcon tube were shaken for 30 s and then centrifuged at 13,000 rcf for 10 min at room temperature, resulting in a two-phase formation where the aqueous upper phase was carefully transferred into a fresh 15 mL falcon tube. The phenol:chloroform:isoamyl alcohol addition, as well as the centrifugation step, was repeated. The upper phase was retrieved and transferred into a fresh 15 mL falcon tube. Next, one volume of chloroform:isoamyl alcohol (24:1) was added and shaken for 30 s, followed by centrifugation at 13,000 rcf for 10 min at room temperature. The upper phase was transferred into a fresh falcon tube where two volumes of ice-cold 100% ethanol and 1/10 of sodium acetate 3.0 M pH 5.3 were added. The samples were left overnight at −20 °C to allow DNA precipitation. A centrifugation step at 4 °C was performed the following day, and the supernatant was discarded. The DNA pellets were washed with 80% ice-cold ethanol and resuspended in ultra pure nuclease-free water (Ambion). The extracted DNA was quantified with a Qubit 3.0 Fluorometer (Thermo Fischer Scientific) using a Qubit dsDNA High Sensitivity range assay kit (Thermo Fischer Scientific). At the same time, the quality of the resulting DNA was assessed by 1% agarose gel electrophoresis.

Preparation of 16S rRNA gene amplicon library, sequencing and analysis To gain an initial, rapid overview of the microbial community and confirm the presence of a bacterial stratification along the BSI [40] and Campylobacterota members, we performed 16S rRNA gene amplicon sequencing on the 12 samples (two seawater, nine BSI and one brine body). The bacterial 16S rRNA gene region V3-V4 was amplified via PCR using the primers 341F 5'-CCTACGGGNGGCWGCAG-3' and 785R 5'-GACTACHVGGGTATCTAATCC-3' [41] and amplicon library was prepared following the method described in Additional file Method S1. Samples were sequenced using a 300 bp paired-end protocol on the Illumina MiSeq platform in the Bioscience Core Lab (BCL) at KAUST. The 16S rRNA gene raw reads from MiSeq were analysed using the DADA2 pipeline [42] integrated into the QIIME2 pipeline v2024.2.0 [43], as detailed in Additional file Method S1. Briefly, the analysis involved quality filtering, trimming of sequencing adapters, and removal of chimeric sequences. Paired-end reads were merged, and error correction was applied to generate Amplicon Sequence Variants (ASVs). Taxonomy was assigned using the reference SILVA v138.1 database [44].

Metagenomic library preparation, sequencing and analysis The metagenomic libraries were constructed from the 11 samples (one seawater, nine BSI and one brine body) using the Ovation Ultralow V2 DNA-Seq Library preparation kit (NuGen) as previously described [40]. Briefly, a range of 50–100 ng of DNA from each fraction was diluted in 120 µL of ultra-pure water (Ambion) in a Covaris snap cap microtube (PN 520045, Covaris). The DNA fragmentation was performed by Covaris M220 sonication to acquire 300 bp DNA fragments using a modified sonication protocol: 70 s treatment time, 200 cycles per bust, 20% duty factor, 50 W peak incident power. The fragmented DNA was end-repaired, tagged with a univocal index for each sample, randomly amplified, and cleaned with AMPure XP Beads (Beckman Coulter) following the NuGen library preparation protocol. The quality of the libraries was assessed by Bioanalyzer 2100 (Agilent). The DNA was quantified with a Qubit 3.0 dsDNA high-sensitivity quantification assay kit, and the libraries were pooled into a final 20 nM pool. The pool quality was assessed again by Bioanalyzer 2100 (Agilent) and qPCR with Kapa Library Quantification kit (KAPA Biosystems). The sequencing was performed as 150 bp paired-end reads using the Illumina HiSeq 4000 platform at BCL (KAUST). Metagenomes' raw reads were demultiplexed and subjected to an initial quality control by FastQC v0.12.1 to evaluate the sequence depth. Raw reads were then analysed with SingleM v14.0 (https://github.com/wwood/singlem) to quantify the relative abundance of bacterial taxa. We utilised the ribosomal protein gene *rpsB* clustered at 95% identity to create a metagenome-based operational taxonomic unit table (Additional file Data S1). After this, raw reads were further processed to trim adapters and low-quality bases by the wrapper script Trim Galore v0.6.10 (https://github.com/FelixKrueger/TrimGalore) that combines cutadapt and FastQC v0.12.1 software [45–48]. The resulting reads from the 11 metagenomes were individually assembled into contiguous sequences (contigs) using MEGAHIT v1.2.9 [49] within the MetaWRAP v1.3 pipeline. We opted to individually assemble the metagenomes along the BSI to evaluate whether spatial or environmental variations in the composition and metabolic potential of Campylobacterota occur across different points along the gradient [50]. Following assembly, the contigs were binned into genome bins using three independent

binning tools: MaxBin2 v2.2.6, MetaBAT2 v2.12.1, and CONCOCT v1.0.0 [51–54] to enhance assembly quality and improve the accuracy of downstream analyses [55, 56]. A schematic representation of the assembly and binning approach employed is reported in the Additional file Fig. S3. The assembly quality of each bin was assessed using QUAST v5.2 [57], and their reconstruction quality was evaluated using CheckM v1.0.9 [58] and CheckM2 v1.0.2 [59]. We designated as metagenome-assembled genomes (MAGs) all the bins that showed completeness greater than 75% and contamination less than 10%. MAGs were assigned to taxonomic classifications based on the Genome Taxonomy Database (GTDB) v2.3.2 using the GTDB-Tk toolkit with the full_tree option [60, 61]. To remove redundancy among MAGs, dereplication was performed using the dRep v3.5.0 tool [62] with default settings (ANI of 95%, 10% minimum aligned fraction, 75% completeness, hierarchical clustering using average linkage). For each ANI cluster, dRep evaluates genome quality by scoring completeness and contamination (based on CheckM) and selects the genome with the highest score within each cluster. This scoring method prioritises genome quality, keeping the most complete and least contaminated genome as the representative for each cluster. The relative abundances of the dereplicated MAGs were quantified across the seawater, BSI and brine body by mapping back the filtered metagenomic sequences to the MAGs using BBMap v38.90 [63] with default parameters.

Phylogenomic analysis of Campylobacterota Among the dereplicated MAGs, three genomes were phylogenetically classified by GTDB within the Campylobacterota phylum [64] (homotypic synonym *Epsilonproteobacteria* class [4]). Phylogenomic trees of *Sulfurimonas* and *Sulfurovum* genera were built using GToTree v1.8.4 [65] and GTDB-Tk v2.4.0, based on Hidden Markov Models (HMMs) [66] that rely on single-copy marker gene sets present in a recent tree of life that covers all three domains. Genes from each genome are called with Prodigal v2.6.3 [67], followed by marker genes identification and alignment using HMMER v3.3.2 [68] to create a multiple sequence alignment. A maximum likelihood tree was then generated using FastTree2 after 1000 permutations [69] and visualised in iTOL [70]. The *Sulfurimonas* and *Sulfurovum* genomes selected for the phylogenomic trees include (i) type strains that are available on the List of Prokaryotic names with Standing in Nomenclature (LPSN) database, (ii) MAGs assembled from less-saline deep pools in the Mediterranean Sea [33], and (iii) genomes (primarily MAGs) from the latest version of GTDB (Release 09-RS220). Average nucleotide identity (ANI) [71], digital DNA-DNA hybridisation (dDDH) [72], percentage of conserved proteins (POCP) [73] and average amino acid identity (AAI) metrics were further computed to assess the similarity between/among Kebrit Deep MAGs and the genomes of the related species (type strains and MAGs) by using JSpeciesWS (https://jspecies.ribohost.com/jspeciesws) [71], GGDC v3.0 (genome-genome distance calculator; https://ggdc.dsmz.de), DIAMOND v2.1.9 (https://github.com/bbuchfink/diamond) after Prokka v2.3.0 [74] proteins annotation, and EzAAI pipeline [75], respectively.

Sulfurimonas and *Sulfurovum* pan-genome analyses

Through pan-genome analyses, we aimed to identify metabolic traits and adaptations encoded by *Sulfurimonas* and *Sulfurovum* that are potentially crucial for survival and functionality in the sulfidic, high-saline marine deep-sea environments of DHABs. As well, we seeked to pinpoint features that differentiate these genomes from those of their closest type species and relatives from similar sulfidic marine environments, such as deep pools and vents. To assessed it, we included in the pan-genomes the genomes of (i) Kebrit Deep Campylobacterota MAGs (Kbt_01, Kbt_02 and Kbt_03), (ii) all high-quality *Sulfurimonas* and *Sulfurovum* MAGs reconstructed from the Mediterranean deep-sea pools whose salinity ranges from 40 to 60 PSU [33], (iii) high-quality, closely related genomes from sulfidic deep-sea environments, such as water/sediment from hydrothermal vents, because bacteria in these habitats experience selective pressures similar to those in our DHABs, with the exception of salinity, and (iv) closest-related type species—independently from their environment of origin—as representatives of the two genera to provide biological and taxonomic context. Accession IDs of the selected genomes and information on their origin/isolation are provided in the Additional file Table S1. Notably, considering the computational basis of the pan-genome analysis, the inclusion of other genomes would inevitably increase the number of genes, as previously observed in the case of *Sulfurimonas* [2, 24, 76] and *Sulfurovum* [77], altering the proportion of genes categorised into the different categories [24]. The selected genomes were analysed using the pan-genome workflow in anvi'o v8 [78]. The pangenome analysis was conducted with the following parameters: a minimum bit-score threshold (-min-bit) of 0.5, an MCL inflation parameter (-mcl-inflation) of 10, and the exclusion of partial gene calls to focus on high-confidence gene clusters. Gene clustering was based on amino acid sequence similarity, applying the Markov Cluster Algorithm (MCL), which groups genes into homologous clusters based on sequence similarity. For each genome, gene clusters were identified, and their presence/absence across genomes was determined. The resulting gene clusters were categorised into core

(present in all genomes), accessory (present in more than one genome but not in all), and specific (present only in one genome). Results were visualised using the anvi-display-pan, which provided a graphical representation of gene cluster distribution across genomes. Functional annotation of gene clusters was done using the KEGG and COG databases integrated within anvi'o that assign KO (KEGG orthology) and COG identifiers, respectively.

Gene annotation and metabolic potential of *Sulfurimonas* and *Sulfurovum* genomes

All Kebrit Deep bacterial MAGs (3 Campylobacterota and 77 non-Campylobacterota), along with genomes of related species within *Sulfurimonas* and *Sulfurovum* genera (Additional file Table S1), were further annotated to get insight into their metabolic potential. Prokka v2.3.0 [74] was initially employed for gene discovery through prodigal [67] and protein annotations. To further dissect the key functions and main metabolic pathways, proteins were annotated using eggNOG v5.0 [79] and METABOLIC v2.0 [80]. Isoelectric points of proteins from genomes were also determined by the IEP software in the EMBOSS suite v6.6.0.0 [81].

Co-occurrence network depicting interactions between bacteria in the community of Kebrit Deep BSI To investigate potential interactions among/within Campylobacteria (3 MAGs) and the other bacterial community members (77 MAGs) in the Kebrit Deep BSI, we constructed a proportionality-based co-occurrence network using the R package *propr* [82]. Unlike conventional correlation analyses, which can introduce biases when applied to compositional data (e.g., relative abundance matrices), proportionality metrics are specifically designed to account for the constant-sum constraint and avoid spurious associations resulting from data compositionality [83]. We used the proportionality metric rho (ρ) to define pairwise interactions between MAGs. Both positive (co-occurrence) and negative (mutual exclusion) interactions with ρ-values greater than |0.8| [84] were plotted using Gephi v0.10.1 [85], applying the Force Atlas layout with default settings to optimise the positioning of nodes (i.e., MAGs) and edges (interactions). The co-occurrence network statistics were calculated using the same software, including the number of modules, referring to those groups of nodes that are more strongly connected, the average cluster coefficient, referring to the proportion between node-neighbours connections and the total possible connections of the node with their neighbours, and the average path length, referring to the average number of steps required to travel between all pairs of nodes in the network, which indicates how connected/compact the network is.

Results and discussion

Microbial diversity along the BSI gradient of Kebrit Deep The sampling strategy applied in our study allowed us to obtain a fine spatial separation of the BSI gradient of the Kebrit Deep (Fig. 1B, C, Additional file Figs. S1 and S2). The BSI presents high levels of H_2S (~150–527 µM) [36], high CO_2 concentrations (4630 µM), and small amounts of N_2, methane, and ethane compared with other deep-sea DHABs of the Red Sea [86–88]. Salinity gradually increases from 40.9 PSU in the seawater to 218.4 PSU in the brine body, with a consistent upward trend of ~8 PSU every ~10 cm (Fig. 1C, Additional file Table S2). pH decreases along the BSI from 8.2 in the seawater to 6.0–5.8 in the BSI and 5.4 in the brine body, while temperature ranges from 21.5 °C to ~ 23.2 °C and oxygen from ~2.4 to 0.3 mg/L (Fig. 1C, Additional file Table S2). Such physico-chemical gradients determine a stratification of the microbial communities (Additional file Fig. S4) similar to what is observed in the BSI of other DHABs [1, 10, 40]. The read-based approach initially employed to assess the relative abundance of bacteria (Additional file Data S1) showed that in addition to Cloacimonadota (average relative abundance of 28%) and Paceibacterota (17%), members of the Campylobacterota make up an average of 5% of the total BSI bacterial community, ranging from 9.1% in the upper BSI layer (~91 PSU) to 3% in the lower BSI layer (~155 PSU) (Additional file Fig. S4). In contrast, Campylobacterota represented only 0.2% and 1.5% of the total community in the seawater and brine body, respectively. The stratification of Campylobacterota along the BSI was also detected by our first screening using 16S rRNA gene amplicon sequencing (Additional file 2: Fig. S5, Data S2), even though it showed an overabundance of Campylobacterota, likely due to PCR preferential amplification associated with the use of universal primers, an issue that does not affect metagenomic sequencing.

Metagenomic assembly, binning, and identification of Campylobacterota A MAG approach was applied to reconstruct genomes of microorganisms associated with Kebrit Deep DHAB. High-quality sequences from the whole genome shotgun metagenomes were individually assembled, generating 6,333,803 contigs, with a total length of 5089 Mbp and an average *N50* value of 1904 bp (Additional file Data S3). Binning of assembled contigs followed by dRep dereplication resulted in 111 non-redundant, medium/high-quality MAGs (i.e., ≥ 75% completeness and ≤ 5% contamination), of which 80 were assigned to bacteria (Additional files Fig. S3B, Data S4A). Among the dereplicated bacterial MAGs, three were identified as Campylobacterota, namely Kbt_01, Kbt_02 and Kbt_03 (ANI values > 99.5% for the 25, 15 and 14 genomes within the three clusters, Additional file Fig. S6). ANI values among the three Campylobacterota

MAGs (range, 65.7–79.9%) indicated that they represent three different bacterial species [73, 89], while POCP values (49.7–70.9%) showed that two of them, Kbt_02 and Kbt_03, belong to the same genus [72, 73, 90] (Additional file Table S3). GTDB-Tk classification placed them in two distinct genera: Kbt_01 within *Sulfurimonas* and Kbt_02 and Kbt_03 within *Sulfurovum* (Additional file Data S4A). The three MAGs reached up to 8.9% of the microbial community recovered along the BSI layers (Fig. 1D, Additional file Data S4B). *Sulfurovum* Kbt_02 had the highest relative abundance among the three, ranging from 5.1% in the upper part to 2.2% in the lowest BSI layer, while *Sulfurimonas* Kbt_01 and *Sulfurovum* Kbt_03 displayed similar relative abundance throughout the interface with a maximum of 2.1% and 1.8%, respectively, in the upper portion of the BSI to less than 1% in the lowest BSI layer (Fig. 1D). The three MAGs covered nearly the entire diversity of Kebrit Deep' Campylobacterota, leaving only a small amount of reads not reconstructed within the genomes of this phylum (relative abundance, 8.9% from MAGs vs 9.1% from SingleM read-based approach). Given that, we cannot exclude that other Campylobacterota genomes could be assembled with deeper sequencing efforts or other metagenomic tools in the future.

Phylogenomic analysis reveals novel *Sulfurimonas* and *Sulfurovum* species in the BSI of Kebrit Deep

Phylogenomic trees based on 120 concatenated genes were computed (Fig. 2A, Additional file Figs. S7 and S8) to compare the three dereplicated genomes from Kebrit Deep with those of known *Sulfurimonas* and *Sulfurovum* species, including genomes of type species and MAGs from Mediterranean deep-sea pools, hydrothermal vents, geothermal sediments, and coastal environments (Additional file Table S1). Kbt_01 had *Sulfurimonas marina* B2^T from deep-sea sediments as the closest related species, and together, they grouped with *Sulfurimonas* entries inhabiting deep-sea hydrothermal vents. The two MAGs Kbt_02 and Kbt_03 clustered in the *Sulfurovum* genus in a branch including *Sulfurovum mangrovi* ST1-3^T and two MAGs assembled from geo-hydro-thermal habitats, with Kbt_03 as the most distant. Notably, *Sulfurimonas* and *Sulfurovum* MAGs assembled from the small Mediterranean Sea deep pools clustered apart from the Kebrit Deep MAGs (Fig. 2A, Additional file Figs. S7 and S8), indicating that the different chemistry and the high salinity of the Kebrit Deep have favoured the establishment/persistence of different genotypes. The taxonomic relationship of *Sulfurimonas* Kbt_01 and *Sulfurovum* Kbt_02 and Kbt_03 with their related genomes was further clarified by computing the ANI, dDDH, POCP and AAI values. While in the case of ANI and dDDH, all comparisons resulted in values lower than the species-level delineation threshold (95–96% and 70%, respectively; Table 1, Additional file Data S5), POCP and AAI for genus delineation had values higher than the respective threshold (Additional file Data S5).

These results and the phylogenetic placement of the Campylobacterota MAGs of the Kebrit Deep (Fig. 2A) support the occurrence of previously uncharacterised species of the genera *Sulfurimonas* (Kbt_01) and *Sulfurovum* (Kbt_02 and Kbt_03). According to the standards outlined in the International Code of Nomenclature of Prokaryotes (ICNP) for microbial uncultivated species and considering that the MAGs have completeness 97.5%, 98.2% and 93.4%, respectively, and contamination < 1.5%, we propose to classify Kbt_01, Kbt_02 and Kbt_03 into the novel candidate species *Candidatus* Sulfurimonas kebritiensis, *Candidatus* Sulfurovum kebritense and *Candidatus* Sulfurovum profundilacunae, respectively.

(See figure on next page.)

Fig. 2 Phylogenomic and pan-genome analyses of reconstructed Campylobacterota MAGs from Kebrit Deep BSI. **A** Phylogenomic tree encompassing *Sulfurimonas* and *Sulfurovum* genomes (isolates and MAGs) made using GToTree [56] and a set of 120 bacterial marker genes. Details of the used genomes are reported in Additional file Table S1. *Caminibacter mediatlanticus* TB-2^T (GCA 00584398) is added as an outgroup to ensure the robustness of phylogenetic affiliations. Bootstrap values are based on 1000 replicates; only values above 50% are shown at branch nodes (refer to circle size). Scale bar refers to a phylogenetic distance of 0.1 nucleotide substitutions per site. MAGs obtained in the present work (Kbt_01, Kbt_02 and Kbt_03) are reported in bold. Colours define the original environment from where the genomes were sequenced/assembled. **B** and **C** Pan-genomes of *Sulfurimonas* and *Sulfurovum* genera include the genomes of MAGs assembled from Kebrit Deep BSI, those from the less-saline Mediterranean Sea deep pools, and those from the closest related type species and MAGs identified by phylogenomic analysis (**A**). Pan-genome plots display gene clusters detected in Kebrit Deep MAGs Kbt_01, Kbt_02 and Kbt_03 in green, orange and light-blue, respectively, while those detected in the other reference genomes in black; light-shades of these colours indicate the absence of the gene clusters. In each plot, core gene clusters, which consist of those gene clusters present in all individuals within the group, are indicated by a blue line; Kbt_01, Kbt_02 and Kbt_03 specific gene clusters are also reported using the colour code described above. Functional annotation of gene clusters is reported in Additional File Data S6

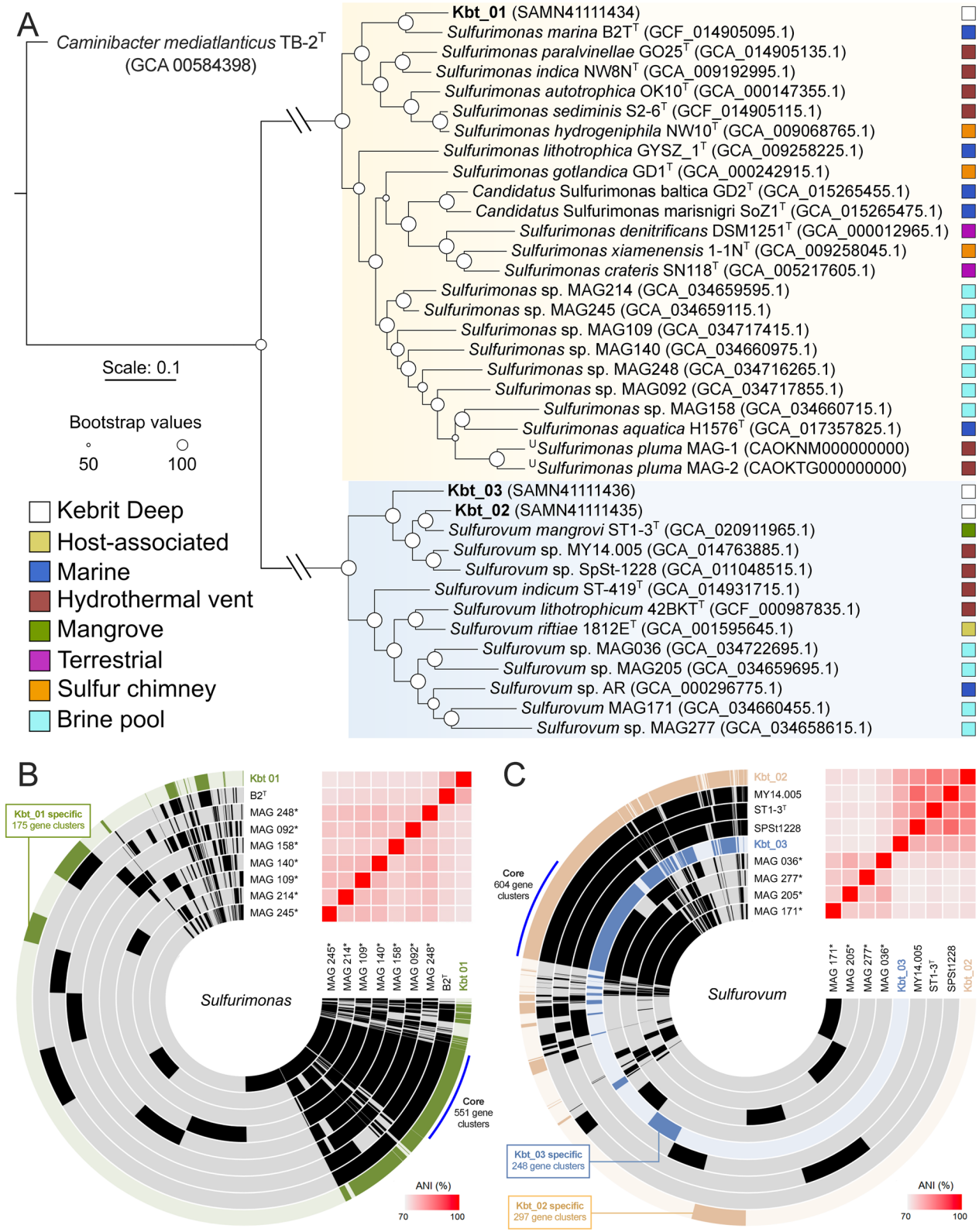

Fig. 2 (See legend on previous page.)

Table 1 Genomic average nucleotide identity (ANI) values of *Sulfurimonas* sp. Kbt_01 and *Sulfurovum* spp. Kbt_02 and Kbt_03 against the genomes of their closest related type species and MAGs (marked with an asterisk [*]) based on the phylogenomic tree (Fig. S2A), and high-quality MAGs assembled from Mediterranean Sea deep pools

ANI (%)	Kbt_01	B2^T*	MAG092	MAG248	MAG158	MAG140	MAG109	MAG214	MAG245
Kbt_01	/								
B2^T*	77.94	/							
MAG092	70.71	71.40	/						
MAG248	71.01	71.82	74.81	/					
MAG158	70.73	71.64	74.69	73.71	/				
MAG140	70.55	71.73	74.71	75.91	73.29	/			
MAG109	70.95	72.13	75.35	75.41	73.45	76.94	/		
MAG214	70.68	72.19	73.91	74.59	73.05	76.24	75.86	/	
MAG245	70.07	70.96	74.02	74.56	72.54	75.48	76.18	74.79	/
ANI (%)	**Kbt_02**	**Kbt_03**	**ST1-3^T***	**MY14.005***	**SpSt-1228***	**MAG171**	**MAG205**	**MAG036**	**MAG277**
Kbt_02	/								
Kbt_03	77.94	/							
ST1-3^T*	85.04	77.59	/						
MY14.005*	82.08	77.32	82.48	/					
SpSt-1228*	81.67	77.16	81.78	86.81	/				
MAG171	70.53	70.17	70.75	69.94	69.95	/			
MAG205	70.64	69.91	70.54	69.49	69.49	73.4	/		
MAG036	72.01	71.77	72.01	71.28	71.31	74.23	77.85	/	
MAG277	70.19	69.58	70.19	69.48	69.36	73.66	74.11	73.98	/

Specifically, *Sulfurimonas* sp. Kbt_01 MAG is compared to *S. marina* B2^T and Mediterranean Sea deep pools' MAGs (MAG092, MAG248, MAG158, MAG140, MAG109, MAG214, and MAG245). *Sulfurovum* spp. Kbt_02 and Kbt_03 MAGs are compared to the closest relatives *S. mangrovi* ST1-3^T, MAGs MY14.005 and SpSt-1228, and Mediterranean Sea deep pools' MAGs (MAG171, MAG205, MAG036, and MAG277). Details on reference genomes are reported in Additional file Table S1. Comparisons with other genomes of related type species and MAGs within the *Sulfurimonas* and *Sulfurovum* are reported in Additional file Data S5

Genome-related statistics of *Sulfurimonas* and *Sulfurovum* MAGs

Genome-related statistics showed that the dereplicated high-quality MAGs Kbt_01, Kbt_02 and Kbt_03 have genomes of 1,874,159 bp (97.5% completeness), 2,210,531 bp (98.2% completeness) and 1,794,780 bp (93.4% completeness), respectively (Additional file Data S4C). These genomes were smaller than those of their closest cultivated relatives, namely *S. marina* B2^T for Kbt_01 and *S. mangrovi* ST1-3^T for Kbt_02 and Kbt_03, with reductions of ~0.387 Mbp for Kbt_01, ~0.761 Mbp for Kbt_02 and ~1.176 Mbp for Kbt_03. Notably, even if an additional 2–7% increase in genome size is assumed to reach 100% completeness, it is unlikely that the genome size of Kebrit Deep MAGs would be significantly larger than those of related species. However, when considering the average size of more distant related genomes, only Kbt_03 still showed a consistent, remarkable reduction in the genome size (range reduction, 0.080–0.567 Mbp). The overall observed genome reduction was associated with a high coding density (i.e., the proportion of the genome comprising coding sequences): values range from 0.905 in Kbt_03 to 0.930 in Kbt_02 and 0.949 in Kbt_01. High coding density typically indicates a streamlined (efficient) genome, possibly suggesting a higher level of metabolic interdependency with other members of the community [40] to support the efficient use of nutrients, especially where they are limiting [2, 91]. The genomes of the three novel Campylobacterota from Kebrit Deep BSI also presented a GC content (39.5%, 44.2% and 44.8% in Kbt_01, Kbt_02 and Kbt_03, respectively) higher than several closely related genomes. For instance, Kbt_01 consistently showed higher GC content (+3.6% *vs*. closest related genomes and an average of +5.4% *vs*. other related genomes), while Kbt_02 and Kbt_03 were richer in GC only in comparison to MAGs from Mediterranean deep-sea pools, *S. lithotrophicum* and *S. indicum* (+4.7–9.9% for Kbt_02 and +5.3–10.4% for Kbt_03; Additional file Data S4C). Such differences may be attributed to the isolation imposed by the density barrier of the BSI, which can limit dispersal, as well as to the unique physico-chemical conditions of Kebrit Deep, such as extremely high salinity, which may impact DNA stability [92]. The need to repair DNA damage—induced directly or indirectly by high salt concentrations—can lead to frequent GC-biased gene conversion, resulting in a higher GC content [93, 94].

Gene content variability of *Sulfurimonas* and *Sulfurovum* MAGs

What are the common/specific adaptations of *Sulfurimonas* and *Sulfurovum* in a sulfidic marine hypersaline environment? Does high salinity drive broad genetic divergences or only hyper-salinity-specific adaptations? To answer these questions and identify metabolic traits potentially crucial to survival in DHABs, we computed pan-genome analyses within *Sulfurimonas* and *Sulfurovum* genera, considering Kebrit Deep MAGs (Kbt_01, Kbt_02, and Kbt_03), high-quality MAGs from Mediterranean deep-sea pools (Additional file Table S1), which are the only genomes available from samples with salinity higher than seawater (up to 60 PSU), and Kebrit Deep MAGs' closest related type species and MAGs (Fig. 2A) as reference.

Sulfurimonas pan-genome

The *Sulfurimonas* pan-genome analysis revealed a total of 6,280 gene clusters (Fig. 2B, Additional file Table S4 and Data S6A). Core gene clusters, present across all genomes, accounted for 9% ($n=551$) of the total pan-genome. This core percentage varied between 23% and 35% in individual genomes, with Kbt_01 displaying an intermediate proportion of 29%. Genome-specific gene clusters comprised 56% ($n=3491$) of the overall pan-genome, but in Kbt_01 this category dropped to 9%, the lowest value among the genomes analysed. The remaining 36% ($n=2238$) were identified as accessory gene clusters shared among two or more genomes (Fig. 2B, Additional file Table S4). In Kbt_01, the accessory genes were predominant, representing 60% of its gene content (total gene clusters $n=1876$) (Additional file Table S4). Among these, 13% were shared exclusively with the closest type strain, *S marina* B2^T, while less than 1% were shared exclusively with *Sulfurimonas* MAGs from the less-saline Mediterranean deep-sea pools (Additional file Data S6A). Considering the functionally annotated gene clusters in the *Sulfurimonas* pan-genome (40% annotated via KEGG and 62% via COG, Additional file Data S6A), the core genome included genes encoding carbon fixation through the rTCA cycle, sulfur metabolism pathways (e.g., sulfur carriers, sulfide:quinone oxidoreductase [SQR]), motility (i.e., flagella, twitching motility, chemotaxis, Type IV pilus), and biosynthesis/uptake of proline, an osmoprotectant involved in salinity adaptation [95]. Gene clusters related to the SOX system and cytochrome bd-type oxidase were instead categorised as accessory, as they were detected in Kbt_01 and *S. marina* B2^T but not in all MAGs from the Mediterranean deep-sea pools. Besides the low number of gene clusters specific to Kbt_01, the large portion of unannotated genes prohibit us from identifying the unique metabolic features of Kbt_01, except for the iron complex outer membrane receptor proteins for iron uptake, cytochrome bd-type quinol oxidase with high-affinity for oxygen, and 5-oxoprolinase subunit A implicated in glutamate biosynthesis, another osmoprotectant important for salinity and oxidative stress adaptations [96].

Sulfurovum pan-genome The *Sulfurovum* pan-genome was composed of 5812 gene clusters (Fig. 2C, Additional file Data S6B) that were distributed as 10% ($n=604$) core, 54% ($n=3,118$) genome-specific, and 36% ($n=2090$) accessory clusters, similar to what was observed in the *Sulfurimonas* pan-genome (Additional file Table S4). In the case of Kbt_02 and Kbt_03, the gene clusters within the core category represented 28% and 35%, respectively, while those specific to each genome accounted for 14% plus almost 1% shared by the two. In the accessory category were assigned more than half of the gene clusters detected in Kbt_02 (58%) and Kbt_03 (51%) (Additional file Table S4). While a low percentage of gene clusters were shared exclusively with the type strain *S. mangrovi* ST1-3^T (3% and 1% for Kbt_02 and Kbt_03), Kbt_02 and Kbt_03 had up to 21% and 15% of gene clusters shared with one or more *Sulfurovum* MAGs from Mediterranean Sea deep pools only (Additional file Data S6A). Yet, functional annotation of pan-genome (40% of KO and 59% of COGs) revealed that core gene clusters encoded for primary metabolic functions, such as the rTCA cycle and sulfide:quinone oxidoreductase (SQR) and aerotaxis receptors, as well as for glutamate and glutamine synthesis, which may aid in alleviating salinity stress [96]. SOX system genes were classified as accessory because they were absent in Kbt_03 and only partially present across Mediterranean DHAB MAGs, while CRISPR-Cas system genes were not detected in Kbt_02. Instead, gene clusters specific to *Sulfurovum* Kbt_02 and Kbt_03 included the synthesis of ectoine and hydroxyectoine [97], an additional adaptation to cope with the high salinity of Kebrit Deep DHAB.

As shown by the *Sulfurimonas* and *Sulfurovum* pangenomes, it is plausible to state that the specific conditions of Kebrit Deep BSI have favoured the emergence of adaptive traits that support the proliferation of these Campylobacterota at high salinity, limited nutrients and stratified redox couples along the BSI chemocline.

Metabolic potential of *Sulfurimonas* and *Sulfurovum* MAGs in Kebrit Deep

When analysing the metabolic potential of bacterial MAGs, it is essential to recognise that inferred functions are drawn from genomic annotations and comparative analyses rather than direct biochemical evidence. However, this approach allowed us to assess the functional and adaptation potential of the uncultured Kebrit Deep

MAGs. Specifically, we examined the presence of genes involved in the carbon, sulfur, nitrogen, di-hydrogen (H_2) and iron cycles, as well as those related to motility and adaptation strategies for salinity and osmotic stress (Figs. 3, 4, 5, Additional files Data S7 and S8).

Carbon metabolism and primary production Kbt_01, Kbt_02 and Kbt_03 relied on chemoautotrophic metabolisms, acting as primary producers and thus providing resources for the growth of other microorganisms living in the BSI [3, 4, 98]. This aligns with findings from several microbial metabolic surveys targeting brine and other deep-sea habitats, where Campylobacterota were highlighted as dominant autotrophs [99, 100]. Specifically, the three genomes can fix carbon into an organic form, as indicated by the presence of a complete reverse TCA (rTCA) cycle, typical of *Sulfurimonas* and *Sulfurovum* members [4, 21, 98]. The key enzymes required to perform the rTCA cycle were indeed present in all the genomes, including 2-oxoglutarate:ferredoxin oxidoreductase (*oorABCD*: KEGG codes, K00174-K00177), two variants of the anaerobic pyruvate:ferredoxin oxidoreductase (i.e., *por* [K03737] in *Sulfurimonas* Kbt_01 and *porABCD* [K00169-K00172] in *Sulfurovum* Kbt_02 and Kbt_03), and ATP-dependent citrate lyase (*acl*, K15230). Despite *oor* and *por*/*porABCD* genes being typically highly O_2 sensitive due to their easily oxidable iron-sulfur clusters [101], it has been shown that the production of stress defence relative proteins, such as periplasmic Cu/Zn-binding SOD and a cytoplasmic catalase, support Campylobacterota adaptation to well-oxygenated high-productivity niches, including coastal systems, deep-sea trenches and hydrothermal vents [102, 103]. Kbt_01 genome also encoded for the pyruvate dehydrogenase *pdhABCD* (K00161, K00162, K00627 and K00382), which converts pyruvate in acetyl-CoA under aerobic conditions, suggesting a higher O_2 tolerance [24]. However, the absence of the Calvin cycle and Wood-Ljungdahl pathway (more energetically favourable under anaerobic conditions) suggested that the rTCA is the sole CO_2 fixation pathway utilised by the *Sulfurimonas* and *Sulfurovum* in the Kebrit Deep BSI. This aligns with the literature, which identifies the rTCA cycle as the primary carbon fixation pathway in Campylobacterota, although horizontal gene transfer can occasionally lead to the acquisition of alternative carbon fixation pathways [27]. The autotropic lifestyle of Kebrit Deep MAGs was supported by the absence of key enzymes for heterotrophic metabolisms, like succinate dehydrogenase (*sdhAB*, K00234 and K00235) and citrate synthase (*CS*, K01647), with the latter being present only in Kbt_02. Additionally, the pentose phosphate pathway was incomplete, lacking the oxidative phase. The detected genes were instead involved in gluconeogenesis, which was complete in all the MAGs (Additional file Data S7 and S8).

Acetate is an important energy source in many ecosystems, functioning as an organic electron donor [23]. In the case of Kebrit Deep, all Campylobacterota MAGs encoded the cation/acetate symporter *actP* (K14393), allowing the conversion of the imported acetate into acetyl-CoA via two pathways: a one-step process mediated by the acetyl-CoA synthetase (K01895) of the ACS pathway or the PTA-ACK pathway involving acetate kinase (*ack*, K00925) and phosphate acetyltransferase (*pta*, K00625) [104]. While Kbt_01 encoded both pathways, Kbt_02 and Kbt_03 only possessed the ACS pathway (Figs. 4, 5, Additional file Data S7 and S8). This indicated that only *Sulfurimonas* Kbt_01 could utilise acetate as a carbon/energy source, even while maintaining an autotrophic lifestyle, as observed in *S. gotlandica* [8, 105]. However, microcosms enriched in *Sulfurimonas* and *Sulfurovum* revealed that labelled acetate did not stimulate the growth of these genera but instead that of other Campylobacterota [106]. Considering the microaerophilic condition of the BSI and the lack of evidence for acetate utilisation as a carbon source by *Sulfurimonas* and *Sulfurovum* from Kebrit Deep, it is more likely that these bacteria were autotrophic and use acetate as an alternative electron donor for intracellular metabolic processes. Interestingly, all three MAGs encoded hexosaminidase, an enzyme involved in the breakdown of complex carbohydrates, such as chitin polymers produced by BSI fauna (e.g. copepods and their pre-adult stages) [107]. The chitin oligomers and their monomeric unit, N-acetylglucosamine, could then be further metabolised by the other members of the BSI community via glycolysis and other pathways, providing energy for bacterial

(See figure on next page.)

Fig. 3 Metabolic pathway in *Sulfurimonas and Sulfurimonas* Kebrit Deep MAGs. Presence/absence of genes involved in the energetic metabolic pathways encoded by the genomes of MAGs *Sulfurimonas* Kbt_01, *Sulfurovum* Kbt_02 and *Sulfurovum* Kbt_03 assembled from Kebrit Deep BSI, those from the less-saline Mediterranean Sea deep pools (*Sulfurimonas* MAG 092, MAG 109, MAG 140, MAG 158, MAG 214, MAG 245 and MAG 248; *Sulfurovum* MAG 036, MAG 171, MAG 205 and MAG 277), and those from the closest related type species and MAGs identified by the phylogenomic analysis (*Sulfurimonas marina* B2^T, *Sulfurovum mangrovi* ST1-3^T, and *Sulfurovum* MAGs MY14.005 and SPSt1228). Genes involved in carbon, sulfur, and nitrogen metabolisms are reported, along with those encoding osmoprotectants. The presence of these genes in genomes of other related species within the *Sulfurimonas* and *Sulfurovum* genera is reported in Additional file Data S7 and S8

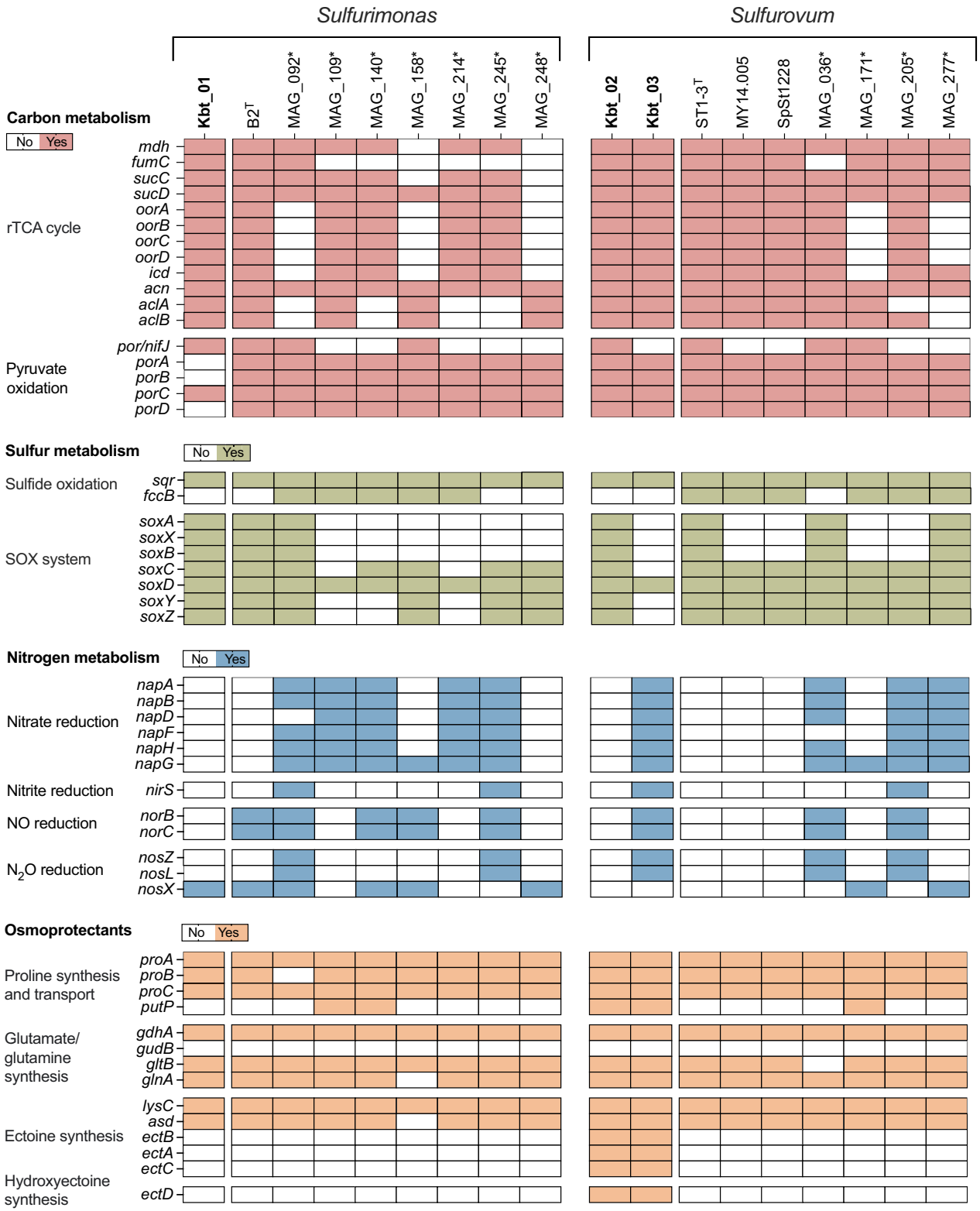

Fig. 3 (See legend on previous page.)

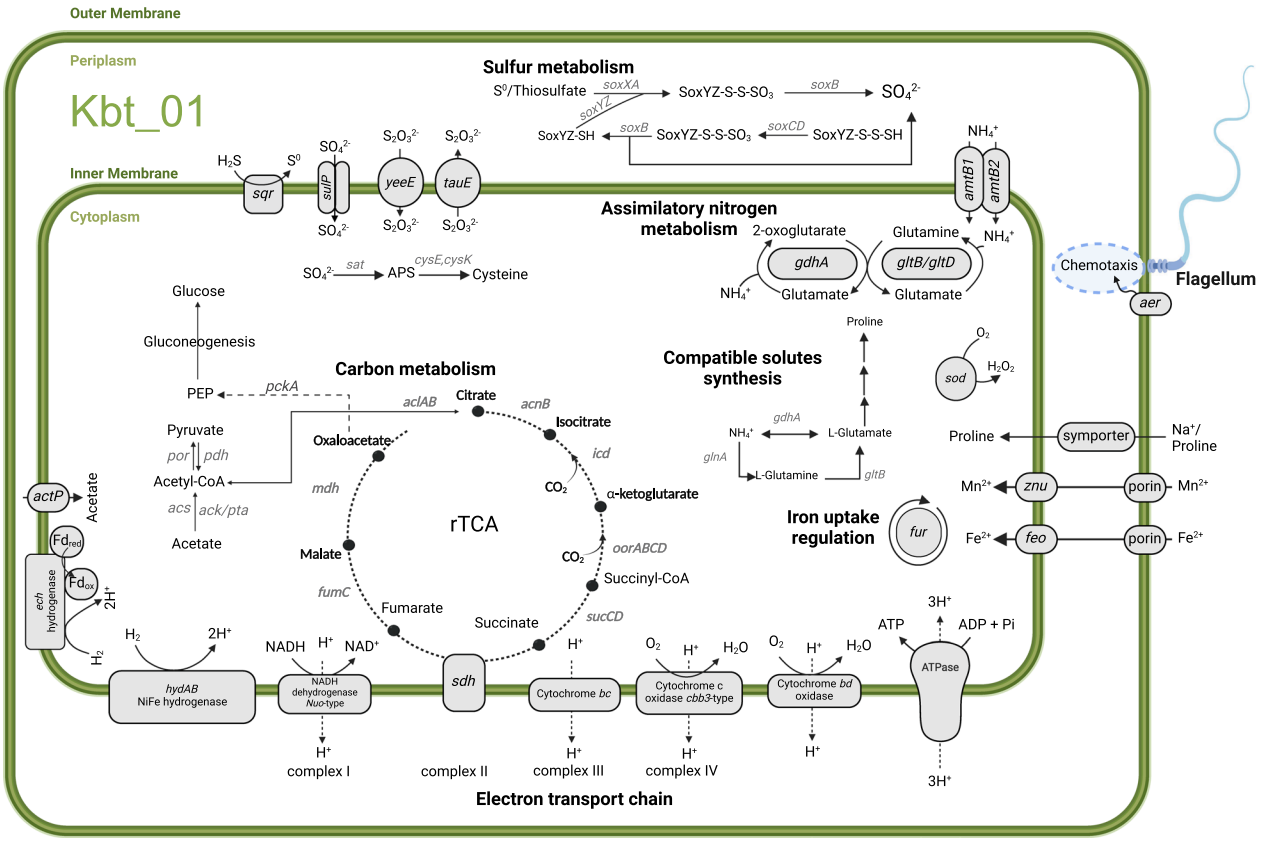

Fig. 4 Metabolic map of *Sulfurimonas* species from Kebrit Deep BSI. Overview of the metabolism inferred from the genome of *Candidatus* Sulfurimonas kebritensis sp. nov. (Kbt_01). The model showcases the presence of genes involved in carbon, sulfur, nitrogen, and iron regulation pathways, hydrogenases, cytochromes, oxygen detoxification mechanisms, transport or biosynthesis of compatible solutes, and motility. Abbreviations of genes are stated in the main text. Created with BioRender.com

growth and contributing to the metabolic continuum of the BSI.

Metabolic redundancy of sulfur metabolism in *Sulfurimonas* and *Sulfurovum* from Kebrit Deep

Sulfur metabolism is a hallmark of the functional and ecological roles of Campylobacterota [108]. In the Kebrit Deep BSI, none of the Campylobacterota genomes possessed genes for dissimilatory sulfate or sulfite reduction pathways. All three genomes had the potential to oxidise sulfide (HS^-) via sulfide:quinone oxidoreductase (SQR, K17218), but none encoded for flavocytochrome c sulfide dehydrogenase *fccB* (K17229) (Figs. 3, 4, 5). *Sulfurimonas* Kbt_01 and *Sulfurovum* Kbt_02 also encoded the pathway for the oxidation of reduced sulfur compounds in the bacterial periplasm via the SOX multienzyme system [109, 110] for which the essential genes are *soxYZ* (K17226 and K17227), *soxA* (K17222), and *soxB* (K17224) [111]. They possess all the genes of this system, except for *soxD* (K22622), detected only by METABOLIC software and not by eggNOG annotation (Additional file Data S7 and S8). However, several variants of the SOX system exist [111], and many sulfur oxidisers possess a "truncated" SOX system lacking *soxCD* genes (K17225 and K22622) [112]. Yet, Kbt_02 had the porin *oprD* (K18093) responsible for the import of elemental sulfur (S^0) in the periplasm and the polysulfide reductase *phsA* (K08352) responsible for the reduction of sulfur in hydrogen sulfide. These genes were absent in Kbt_01 and other reference genomes, suggesting that S^0 uptake may occur via an alternative pathway or it permeates into the cell as H_2S, which can then be converted to S^0 by the sulfide reductase *sqr* (K17218) before further oxidation by the SOX system. Assimilatory sulfate reduction was present in all three genomes, with each having *sulP* transporter (K03321) for importing sulfate into the cytoplasm, where it can be assimilated. Among the transporters, *tauE* sulfite exporters (K07090) were present in all the MAGs, while only Kbt_01 also encoded *yeeE* (K07112), which is involved in importing thiosulfate into the cytoplasm [113, 114]. Sulfur compounds can also be used in the assimilatory sulfate reduction pathway for the synthesis

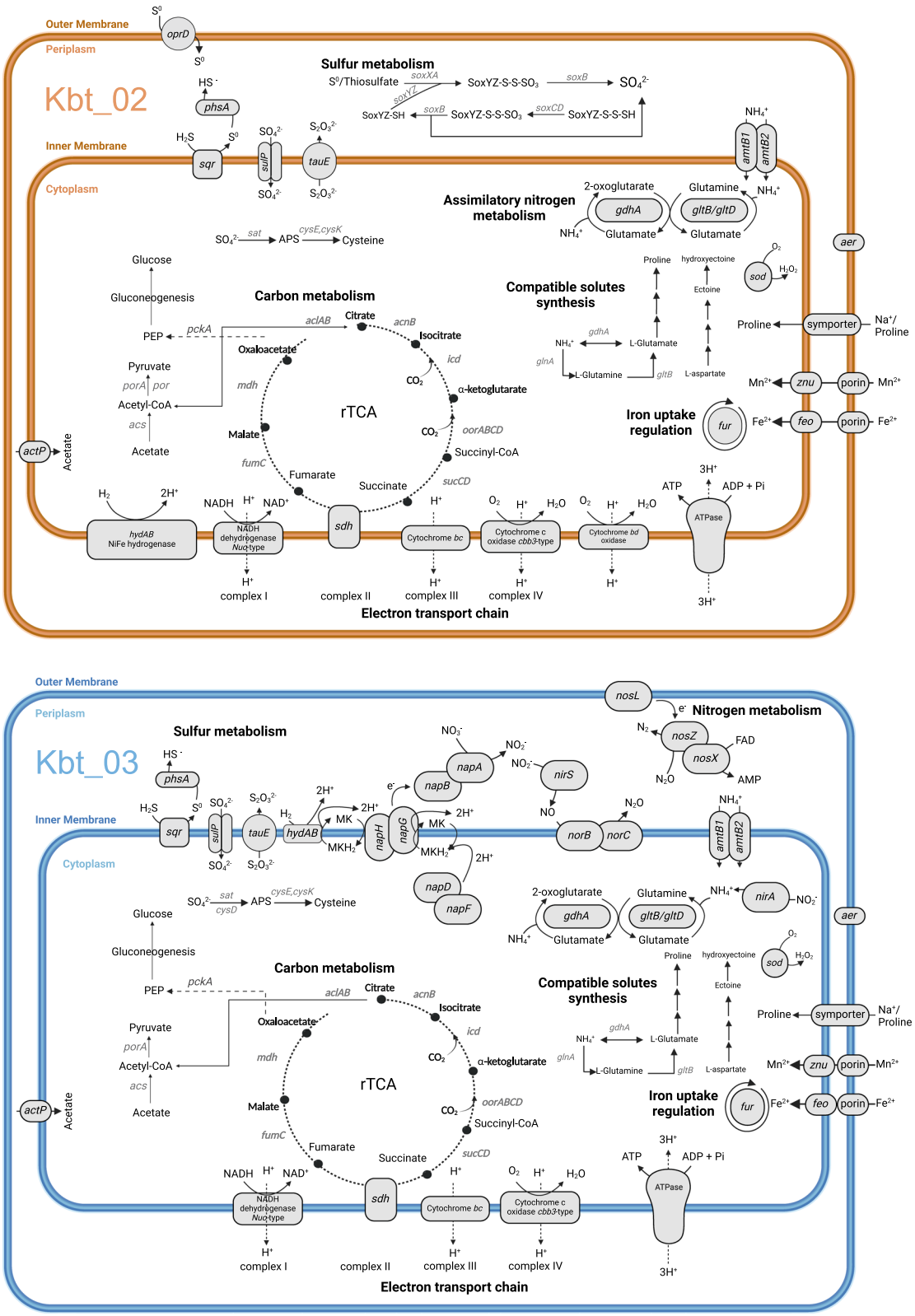

Fig. 5 Metabolic maps of *Sulfurovum* species from Kebrit Deep BSI. Overview of the metabolism inferred from the genome of *Candidatus* Sulfurovum kebritense sp. nov. (Kbt_02, upper cell) and *Candidatus* Sulfurovum profundilacunae sp. nov. (Kbt_03, lower cell). The models showcase the presence of genes involved in carbon, sulfur, nitrogen, and iron regulation pathways, hydrogenases, cytochromes, oxygen detoxification mechanisms, and transport or biosynthesis of compatible solutes. Abbreviations of genes are stated in the main text. Created with BioRender.com

of sulfur-containing amino acids such as cysteine, as indicated by the presence of *sat* (K00958), *cysE* (K00640), and *cysK* (K01738) in the three MAGs and of *cysD* (K00957) in Kbt_03.

Nitrogen metabolism specialisation in Kebrit Deep Campylobacterota The lack of a SOX system in Kbt_03 restricts its ability to exploit sulfur compounds for energy generation, favouring alternative redox couples, such as nitrate (Figs. 3, 5). It displayed all the components required for the denitrification pathway (Figs. 3, 5, Additional file Data S7 and S8), encoding the periplasmic nitrate reductase *napAB* (K02567 and K02568) responsible for the reduction of nitrate to nitrite, cytochrome nitrite reductase *nirS* (K15864) for the further reduction to nitric oxide, the *norBC* reductase (K04561-K02305) to convert NO to N_2O and *nosZ* (K00376), *nosX* (K03734) and *nosL* (K19342) for the conversion of N_2O to N_2 [24] (Additional file Table S5). Additionally, it encoded for the *napD* reductase (K02570) and the ferredoxins *napF* (K02572) and *napGH* (K02573 and K02574), which are involved in the electron transfer required for nitrate reduction and proton extrusion across the cytoplasm. However, all the Kebrit Deep MAGs had the *amtB* gene (K03320) encoding for channel proteins involved in the ammonia uptake and *glt/gdh* genes (K00265 and K00266/K00261) for nitrogen assimilation required for the amino acid metabolism. Kbt_03 also had *nirA* (K00366) encoding ferredoxin nitrite reductase, which converts nitrite to ammonia in the cytoplasm as an alternative way to uptake ammonia. It clearly indicates that while Kbt_03 gains energy relying on dissimilatory nitrate reduction using NO^{3-} as electron acceptor and H_2S as electron donor, Kbt_01 and Kbt_02 only have those nitrogen assimilatory pathways necessary involved in amino acid biosynthesis (Fig. 3).

Hydrogen metabolism The oxidation of H_2 can also be exploited as a possible energy source by all Kebrit Deep Campylobacterota MAGs since they all encoded a group 1 periplasmatic [NiFe]-hydrogenase (K05927 and K05922) (Additional file Fig. S9), which in previous studies has been indicated to support the growth of *Sulfurimonas* sp. in the presence of H_2 [2, 115]. The energy is gained by the proton motive force generated across the periplasmic membrane from the oxidation of H_2 to protons and electrons, which are further transferred to quinone complexes [115]. *Sulfurimonas* Kbt_01 also encoded the group 4e hydrogenase (*echABEF*: K14086, K14087, K14090 and K14091), an energy-converting hydrogenase typically presents in pelagic *Sulfurimonas* species like *S. marisnigri, S. gotlandica,* and *S. baltica* [24], further indicating the possibility that H_2 oxidation represents an alternative source of energy for this bacterium in the BSI. For instance, *Sulfurimonas* spp. isolated from marine sediments can grow on hydrogen [116], particularly *S. denitrificans* showed a faster and denser growth on hydrogen than on thiosulfate alone, mainly relying on its periplasmic [NiFe]-hydrogenases under laboratory conditions. Although we do not have a direct quantification of H_2 level along the Kebrit Deep BSI, H_2 may represent an important energy source in DHABs. Hydrogen can indeed be produced as a product of the fermentation of macromolecules, which largely occurs in the most reduced layer of the BSI [117]. The array of hydrogenases encoded in Campylobacterota MAGs indeed suggests they may also exploit H_2 oxidation as an additional energy source.

Oxygen metabolism in the microaerophilic BSI A primary constraint for anaerobic/microaerophile microorganisms is oxygen toxicity since many crucial enzymes are oxygen-sensitive. In the case of Kebrit Deep Campylobacterota MAGs, defensive mechanisms to cope with the oxygen that persists in the upper BSI of DHABs are required [36, 40]. Besides cytochrome complexes 1–3, Kebrit Deep MAGs encoded a cytochrome c oxidase *cbb3* (*ccoNOPQ*, K00404-K00407), serving as a terminal oxidase with a high affinity for oxygen, allowing the growth at microaerophilic conditions (Additional file Fig. S9 and Table S5). The cytochrome c oxidase *cbb3* has been proven to be involved in O_2 detoxification, supporting microbial adaptation to microaerophilic/anaerobic metabolisms [118, 119]. The genomes of Kbt_01 and Kbt_02 additionally encoded a *bd*-type cytochrome (*cydAB*, K00425- K00426), a terminal oxidase with a high affinity for oxygen that can function efficiently at low oxygen concentrations. This is crucial for the adaptation of these bacteria to the microaerobic conditions of the Kebrit Deep BSI and, in the case of Kbt_02, even to the more oxygen-limiting conditions of the brine body (Fig. 1C, D). All Kebrit Deep Campylobacterota MAGs had the aerotaxis receptor *aer* (K03776) involved in the sensing of oxygen, as well as for the *sod* superoxide dismutase (K04564) that protects cells from the damages induced by reactive oxygen species [120]. *Sulfurimonas* Kbt_01 additionally displayed the hemerythrin gene (K07216), which is involved in oxygen detoxification and oxygen detection in microaerophilic conditions [121, 122].

Iron metabolisms Iron regulation is pivotal in cellular homeostasis, particularly in oxygen-deprived environments such as DHABs. Its concentration must be tightly controlled to prevent oxidative stress and toxicity [123]. All the Campylobacterota genomes analysed encode a ferrous iron transport system *feoAB* (K04758 and K04759) and the ferric uptake regulator *fur* (K03711). Upon sensing elevated intracellular iron levels, *fur* modulates gene expression, inhibiting iron uptake genes, including *feoAB*, while promoting the synthesis of iron

storage proteins [123, 124]. Conversely, under low intracellular iron concentration, *fur* releases repression on iron transport systems, leading to the activation of *feoAB* transporters [125]. Furthermore, oxidative stress can arise from an imbalance between reactive oxygen species production and cellular antioxidant defences. Gene *fur* is also implicated in the cellular response to oxidative stress, potentially enhancing the activity of superoxide dismutase SOD [125]. In Kbt_01, the anaerobic transcriptional regulator *fnr* (K01420) was also identified. Acting as an oxygen sensor, *fnr* activates transcription of the *feo* operon in the absence of oxygen, where the expression of *feo* genes increases three-fold compared to conditions of oxygen exposure [126, 127]. The fine regulation of enzymes, which sense the presence of oxygen in the environment, further suggests how the Kebrit Deep Campylobacterota MAGs have adapted their metabolic strategies to gain energy while remaining protected by overexposure to oxygen along the BSI chemocline.

Tolerance to salinity and osmotic stresses In hypersaline environments, the capacity to maintain a balanced osmotic pressure between the cell and the external environment is crucial for the survival of microorganisms [128]. The synthesis and transport of organic and inorganic osmoprotectants/compatible solutes inside the cytoplasm is often used as an adaptative strategy, conferring the capacity to equilibrate the cellular osmotic pressure to that of the external environment [95, 96]. Amino acid-based compatible solute strategies, including the production, transport and accumulation of proline (*proABC*: K00147, K00931 and K00286), glutamate and glutamine (*gdhA* [K00262], *gudB* [K00260], *gltB* [K00265] and *glnA* [K01915]), were detected in all the Kebrit Deep MAGs (Figs. 4, 5, Additional file Table S5), as well as across the other Campylobacterota analysed (Fig. 3). Instead, genes for the biosynthesis of ectoine and hydroxyectoine (*ectABCD*: K06718, K00836, K06720 and K10674) were exclusively found in *Sulfurovum*, Kbt_02 and Kbt_03 (Figs. 3, 4, 5). Besides its energetic demand, the adoption of a compatible solute strategy can be flexibly regulated in response to salinity conditions [128] because it does not imply cytoplasmatic adaptations of all proteins as in the case of the salt-in strategy (see isoelectric point in Additional file Fig. S10). The synthesis of osmoprotectants in Kebrit Deep *Sulfurimonas* and *Sulfurovum* MAGs supports their distribution along the BSI with *Sulfurovum* species—which are the only Campylobacterota species encoding for ectoine and hydroxyectoine discovered, so far—detected in higher abundance than *Sulfurimonas* in the lower layers of the BSI and down to the brine body (Fig. 1D). However, the overall decrease in abundance observed along the salinity gradient suggests that while osmoprotectant adaptations allow survival of *Sulfurimonas* and *Sulfurovum* species under high-salinity, the energetic cost for maintaining a consistent synthesis/concentration likely limits bacterial proliferation.

Motility Kbt_01 is the only Kebrit Deep Campylobacterota that exhibited genes related to flagellum assembly and chemotaxis (Figs. 4, 5), which is consistent with the motility capacity commonly observed across members of the *Sulfurimonas* genus [4]. It suggests that, unlike its non-motile counterparts, Kbt_01 can dynamically adjust its position within the BSI in response to metabolic demands and environmental cues, leveraging its mobility to optimise resource utilisation and thrive in fluctuating environmental conditions. This motility, coupled with chemotactic capabilities and an array of oxygen-sensing and detoxification mechanisms, underlines the metabolic versatility and resilience of Kbt_01 along the BSI.

Overall, our results show that along increasingly reducing conditions of the BSI, Campylobacterota species adopt different metabolic pathways to exploit different energy sources (electron donors/acceptors), allowing their coexistence and reducing competition (Fig. 6). In the upper BSI, where O_2 and NO_3 are available, Kbt_01 and Kbt_02 likely gain energy from sulfide/hydrogen oxidation using only O_2 as the final electron acceptor, while Kbt_03 may exploit NO_3 reduction (Fig. 6, Additional file Table S5). The depletion of these electron acceptors and the increasing reducing conditions along the depth of the BSI explains the reduction in abundance observed for all three Campylobacterota MAGs in the lower BSI layers (Fig. 1D). Yet, even though osmoprotectants can be synthesised, their accumulation might be not sufficient to protect the cells from the high-salinity and osmotic stress of BSI deeper layers.

Microbial interactions in Kebrit Deep BSI and keystone role of Campylobacterota We speculate that to maintain the electron flux along the BSI chemocline, the microbial community needs to preserve members with diverse metabolic capabilities to sustain all the elemental cycles. To assess this, we evaluated the possible interactions between Campylobacterota (3 MAGs) and the other bacterial members (77 MAGs) of the BSI microbial community by using proportionality analyses to define a community co-occurrence network based on MAGs' relative abundance. Considering interacting taxa with absolute ρ-values > 0.80, 75 MAGs (visualised in Fig. 7 as nodes) were included in the co-occurrence network forming 921 interactions (visualised as connection lines between nodes), of which 457 are classified as positive (co-occurrence) and 464 are negative (mutual-exclusion). The bacterial network comprised four modules (Additional file Fig. S11) and showed a high average cluster coefficient (0.74). Such strong local connectivity and cohesion

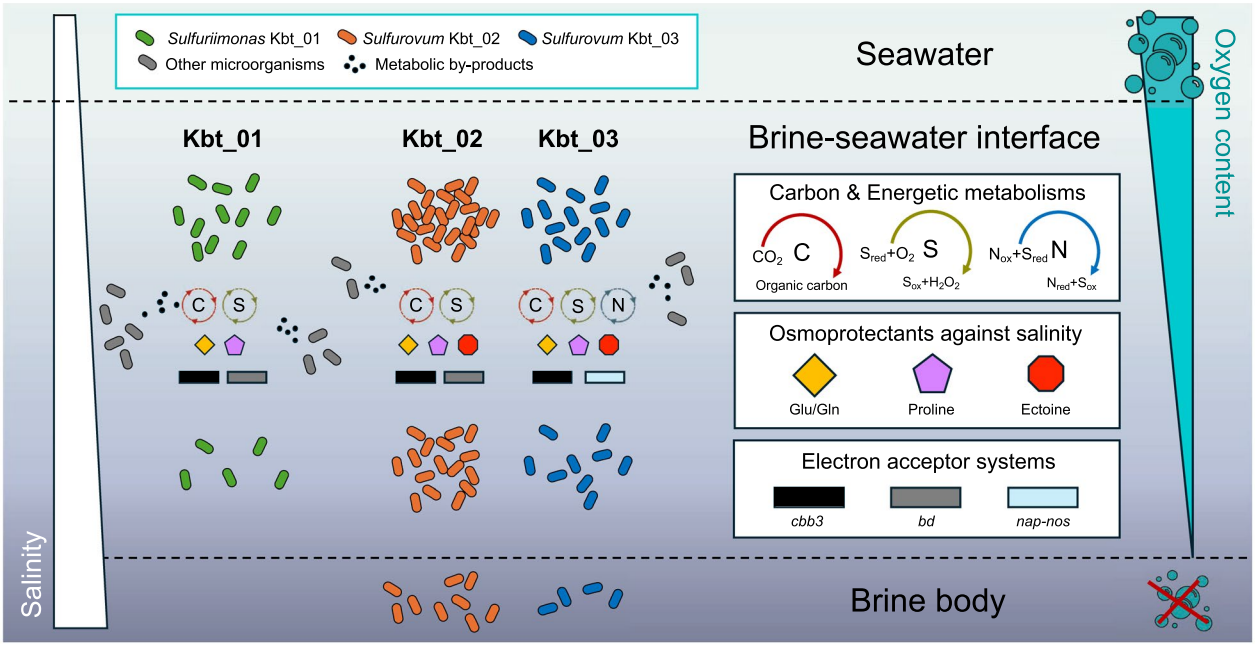

Fig. 6 Model of the distribution, metabolic redundancy and adaptations of Campylobacterota MAGs along the Kebrit Deep BSI. The three Kebrit Deep Campylobacterota MAGs—*Sulfurimonas* Kbt_01 (green), *Sulfurovum* Kbt_02 (orange), and *Sulfurovum* Kbt_03 (blue)—exhibit distinct metabolic and salinity adaptation strategies. Bacterial cells represent their relative abundance along the vertical BSI stratification, with grey cells representing other microorganisms potentially interacting with Campylobacterota and utilising their metabolic by-products (small black dots), such as organic carbon (indicated as C) fixed via rTCA. Kbt_01 and Kbt_02 can gain energy from the oxidation of reduced sulfur forms (indicated as S) using oxygen as the final electron acceptor through pathways involving the SOX system and sulfide:quinone oxidoreductase (SQR). In contrast, Kbt_03 performs nitrate reduction (indicated as N) coupled with sulfur compound oxidation via *sqr* (S) and does not encode for the SOX system. Given the low oxygen concentration along the BSI and in accordance with the energetic metabolisms, the electron transport chain in the three bacteria includes high-affinity cbb3-type (black rectangles) cytochromes for facilitating the reduction of oxygen, even under low oxygen concentrations. Additionally, Kbt_01 and Kbt_02 encode another type of high-affinity cytochromes, the bd-type (grey rectangles), while Kbt_03 encodes periplasmic nitrate reductase (*nap*) and nitrous oxide reductase (*nos*) for nitrate reduction (light-blue rectangle). The decrease in electron acceptors and the increase in salinity along the BSI explain the observed reduction of the abundance of all three Campylobacterota MAGs, but the ability to synthesise osmoprotectants, such as ectoine, alongside proline and glutamate/glutamine (Glu/Gln), enable the two *Sulfurovum* MAGs to persist down to the brine body

between nodes favour the establishment of ecological hubs in which collaborative or synergistic behaviour can enhance network stability. This was further associated with a relatively low average path length (1.89), which implies that most nodes can be reached in less than two steps. The three Campylobacterota—despite representing ~9% of the bacterial community—were involved in 97 interactions, thus representing 10% of the total ones. Specifically, *Sulfurimonas* Kbt_01 and *Sulfurovum* Kbt_02 formed 36 and 38 interactions, respectively, positioning them within the keystone species of the co-occurrence network (third percentile threshold, 34.5; Additional file Data S9), while *Sulfurovum* Kb_03 was involved in 23 interactions only. The analysis of Campylobacterota interactions revealed their extensive connectivity within the microbial community, engaging not only with each other but also with diverse taxa such as Patescibacteria, Marinisomatota, and Pseudomonadota, as well as sulfate-reducing bacteria within the Desulfobacterota group (Fig. 7). Yet, many of these interacting taxa, also act as keystone species within the co-occurrence network, potentially influencing community structure, stability, and resilience. Their presence ensures the maintenance of critical biogeochemical processes and mitigates the impact of environmental fluctuations. Furthermore, the observed metabolic versatility of interacting bacteria (Additional file Data S10) provides additional functional redundancy within the community, a stabilising mechanism that allows communities to sustain essential metabolic processes even under stress or perturbations. It can ensure that key functions, such as sulfur and carbon cycling, persist despite shifts in species composition or environmental conditions.

Conclusion

The physico-chemical conditions of the sulfidic Kebrit Deep BSI—particularly the redox and salinity gradient—define the ecological and metabolic niche available

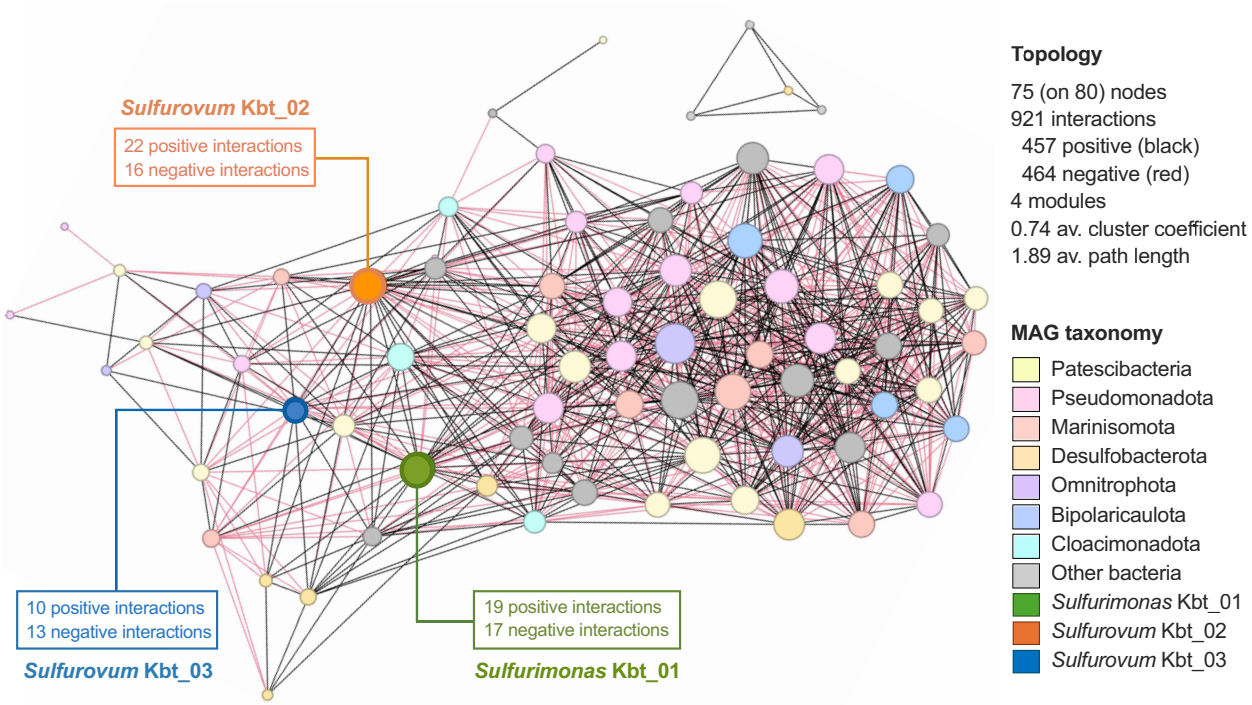

Fig. 7 Bacterial interactions along the metabolic continuum of Kebrit Deep BSI. Visualisation of the co-occurrence network depicting pairwise interactions between bacteria in the Kebrit Deep BSI based on proportionality metric (ρ-values > |0.8|) Nodes represent bacterial MAGs that were retained based on the proportionality threshold selected; they include three Campylobacterota (*Sulfurimonas* Kbt_01, *Sulfurovum* Kbt_02 and *Sulfurovum* Kbt_03) and 72 non-Campylobacterota bacteria (taxonomy is reported in the figure). Edge lines represent the interactions among nodes; black lines indicate positive interactions (co-occurrence), and red lines represent negative interactions (mutual exclusion). The colour and size of nodes correspond to their taxonomic affiliation and number of interactions, respectively. The list of nodes and edges is reported in Additional file Data S9

for microbial colonisation, driving microbial community diversification and dynamics. For example, sulfur-oxidising Campylobacterota are enriched within BSI but are nearly absent in the overlaying seawater. Although H_2S not being a limiting factor for microbial growth along the BSI gradient, it remains intriguing why phylogenetically related bacteria diversify their metabolic strategies despite their overlapping distribution. Our findings reveal that Campylobacterota species across distinct genera, that are *Sulfurimonas* and *Sulfurovum*, display extensive genomic plasticity and metabolic redundancy to efficiently exploit the geochemical gradients and available resources (e.g., reduced sulfur species), supporting ecosystem resilience. At the same time, limiting factors (i.e., electron donors/acceptors) drive metabolic specialisation, as observed in *Sulfurovum* Kbt_03, which can exploit nitrate for energy generation instead of sulfur, reducing competition with other species. However, the overall decrease in the relative abundance of these bacteria due to increasing salinity suggests that the energetic costs associated with synthesising or importing osmoprotectants may surpass their adaptive capacity. Overall, our work underscores the critical role of the BSI chemocline in regulating electron donor/acceptor availability and shaping the metabolic continuum that underpins microbial diversity and interactions in DHABs, as observed for Campylobacterota species.

Description of Candidatus Sulfurimonas kebritensis sp. nov.

Candidatus Sulfurimonas kebritensis (ke.brit.en'sis. N.L. fem. adj. *kebritensis*, pertaining to Kebrit, referring to the Kebrit Deep hypersaline anoxic basin in the Red Sea, from which the genome was first assembled). A member of the phylum Campylobacterota, class *Epsilonproteobacteria*, order *Campylobacterales* and family *Sulfurimonadaceae*. Genome analysis indicates that this halophilic bacterium adopts the compatible solute strategy via the synthesis and import of prolines to cope with salinity. It relies on the oxidation of reduced sulfur species and/or hydrogen to gain energy by using oxygen as an electron acceptor; it possesses oxygen-high-affinity cytochromes (*cbb* and *bd* types). It fixes carbon via rTCA and is motile with genes encoding flagella and chemotactic capability.

Its genome is 1,874,159 bp (completeness 97.5% and contamination 0.8%) with a GC content of 39.5%. It is known from environmental sequencing only. The classification is based on the MLSA phylogenetic comparisons based on 120 conserved genes. The metagenome-assembled genome was deposited in GenBank (accession number SAMN41111434).

Description of Candidatus Sulfurovum kebritense sp. nov.

Candidatus Sulfurovum kebritense (ke.brit.en'se. N.L. neut. adj. *kebritense*, pertaining to Kebrit, referring to the Kebrit Deep hypersaline anoxic basin in the Red Sea, where the genome was first assembled). A member of the phylum Campylobacterota, class *Epsilonproteobacteria*, order *Campylobacterales* and family *Sulfurovaceae*. Genome analysis indicates that this halophilic bacterium adopts the compatible solute strategy via the synthesis of ectoine, hydroxyectoine and proline and the import of proline to cope with high-salinity. It relies on the oxidation of reduced sulfur species and/or hydrogen to gain energy by using oxygen as an electron acceptor; it possesses oxygen-high-affinity cytochromes (*cbb* and *bd* types). It fixes carbon via rTCA and is non-motile. Its genome is 2,210,531 bp (completeness 98.2% and contamination 1%) with a GC content of 44.23%. It is known from environmental sequencing only. The classification is based on the MLSA phylogenetic comparisons based on 120 conserved genes. The metagenome-assembled genome was deposited in GenBank (accession number SAMN41111435).

Description of Candidatus Sulfurovum profundilacunae sp. nov.

Candidatus Sulfurovum profundilacunae (pro.fun. di.la.cu'nae. L. masc. adj. *profundus*, deep; L. fem. n. lacuna, cavity, dip, pool; N.L. gen. n. *profundilacunae*, of a deep pool, referring to the hypersaline anoxic basin in the Red Sea Kebrit Deep, where the genome was first assembled). A member of the phylum Campylobacterota, class *Epsilonproteobacteria*, order *Campylobacterales* and family *Sulfurovaceae*. Genome analysis indicates that this halophilic bacterium adopts the compatible solute strategy via the synthesis of ectoine, hydroxyectoine and proline and the import of proline to cope with high-salinity. It relies on denitrification to gain energy anaerobically by using reduced sulfur species and/or hydrogen as sources of electrons (electron donor); it possesses oxygen-high-affinity cytochromes (*cbb* type). It fixes carbon via rTCA and is non-motile. Its genome is 1,794,780 bp (completeness 93.4% and contamination 1.5%) with a GC content of 44.79%. It is known from environmental sequencing only. The classification is based on the MLSA phylogenetic comparisons based on 120 conserved genes. The metagenome-assembled genome was deposited in GenBank (accession number SAMN41111436).

Abbreviations

DHAB	Deep hypersaline anoxic basin
BSI	Brine-seawater interface
MAG	Metagenome-assembled genome
rTCA	Reverse tricarboxylic acid
PSU	Practical salinity units
CTD	Conductivity, temperature, and depth
DNA	Deoxyribonucleic acid
rRNA	Ribosomal ribonucleic acid
PCR	Polymerase chain reaction
NCBI	National center for biotechnology information
SRA	Sequence read archive
OTU	Operational taxonomic unit
GTDB	Genome taxonomy database
ANI	Average nucleotide identity
dDDH	Digital DNA-DNA hybridization
POCP	Percentage of conserved proteins
AAI	Average amino acid identity
LPSN	List of prokaryotic names with standing in nomenclature
KEGG	Kyoto encyclopedia of genes and genomes
ICNP	International code of nomenclature of prokaryotes
SOX	Sulfur oxidizing
CRISPR	Clustered regularly interspaced short palindromic repeats
SOD	Superoxide dismutase enzymes

Supplementary Information

The online version contains supplementary material available at https://doi.org/10.1186/s40793-025-00669-7.

Additional file 1.

Additional file 2.

Additional file 3.

Additional file 4.

Additional file 5.

Additional file 6.

Additional file 7.

Additional file 8.

Additional file 9.

Additional file 10.

Additional file 11.

Acknowledgements

The authors thank Taskeen Begum and Sadaf Umer for their indispensable help in lab organisation, the Bioscience Core Lab team for their support in sequencing, and the crew of R/V Thuwal and CMOR for their support in sampling the Kebrit Deep brine and BSI. We also thank Professor Aharon Oren for his invaluable help and support on bacterial nomenclature and for explaining the most up-to-date ICNP taxonomy rules.

Author contributions

Conceived and designed the study and experiments: AB, GM and DD. Samples collection: AB and GM. Performed the experiments: RA, AB and GM. Analysed the data: RA, AB, RM, GM and MWVG. Contributed reagents/materials/analysis tools: DD. Wrote the paper: RA, AB and RM. Critically revised the manuscript: GM, MWVG, CO, YC and DD. All Authors read and approved the final manuscript.

Funding
The present study was supported by King Abdullah University of Science and Technology through the baseline research funds of Professor Daniele Daffonchio and the project STABLE (5569-OFP2023).

Data availability
The data that supports the findings of this study are available in the tables and additional files of this article. Sequences were deposited to the Sequence Read Archive of NCBI under the BioProject PRJNA1096827.

Competing interest
The authors declare no competing interests.

Author details
[1]Biological and Environmental Sciences and Engineering Division (BESE), King Abdullah University of Science and Technology (KAUST), Thuwal, Saudi Arabia. [2]Department of Agriculture Forestry and Food Sciences (DISAFA), University of Turin, Grugliasco, Turin, Italy.

Received: 1 July 2024 Accepted: 10 January 2025
Published online: 05 February 2025

References

1. Borin S, Brusetti L, Mapelli F, D'auria G, Brusa T, Marzorati M, et al. Sulfur cycling and methanogenesis primarily drive microbial colonization of the highly sulfidic Urania deep hypersaline basin. Proc Natl Acad Sci. 2009;106:9151–6.
2. Molari M, Hassenrueck C, Laso-Pérez R, Wegener G, Offre P, Scilipoti S, et al. A hydrogenotrophic *Sulfurimonas* is globally abundant in deep-sea oxygen-saturated hydrothermal plumes. Nat Microbiol. 2023;8:651–65.
3. Merlino G, Barozzi A, Michoud G, Ngugi DK, Daffonchio D. Microbial ecology of deep-sea hypersaline anoxic basins. FEMS Microbiol Ecol. 2018;94:fiy085.
4. Waite DW, Vanwonterghem I, Rinke C, Parks DH, Zhang Y, Takai K, et al. Comparative genomic analysis of the class *Epsilonproteobacteria* and proposed reclassification to epsilonbacteraeota (phyl. nov.). Front Microbiol. 2017;8:1–19
5. Waite DW, Vanwonterghem I, Rinke C, Parks DH, Zhang Y, Takai K, et al. Addendum: Comparative genomic analysis of the class *Epsilonproteobacteria* and proposed reclassification to Epsilonbacteraeota (phyl. nov.). Front Microbiol. 2018;9:1–2.
6. Callbeck CM, Lavik G, Ferdelman TG, Fuchs B, Gruber-Vodicka HR, Hach PF, et al. Oxygen minimum zone cryptic sulfur cycling sustained by offshore transport of key sulfur oxidizing bacteria. Nat Commun. 2018;9:1729.
7. Callbeck CM, Canfield DE, Kuypers MMM, Yilmaz P, Lavik G, Thamdrup B, et al. Sulfur cycling in oceanic oxygen minimum zones. Limnol Oceanogr. 2021;66:2360–2392.
8. Grote J, Schott T, Bruckner CG, Glöckner FO, Jost G, Teeling H, et al. Genome and physiology of a model *Epsilonproteobacterium* responsible for sulfide detoxification in marine oxygen depletion zones. Proc Natl Acad Sci. 2012;109:506–10.
9. Fullerton H, Smith L, Enriquez A, Butterfield D, Wheat CG, Moyer CL. Seafloor incubation experiments at deep-sea hydrothermal vents reveal distinct biogeographic signatures of autotrophic communities. FEMS Microbiol Ecol. 2024;100:1–14.
10. Daffonchio D, Borin S, Brusa T, Brusetti L, Van Der Wielen PWJJ, Bolhuis H, et al. Stratified prokaryote network in the oxic-anoxic transition of a deep-sea halocline. Nature. 2006;440:203–7.
11. Mara P, Geller-McGrath D, Edgcomb V, Beaudoin D, Morono Y, Teske A. Metagenomic profiles of archaea and bacteria within thermal and geochemical gradients of the Guaymas Basin deep subsurface. Nat Commun. 2023;14:7768.
12. van der Wielen PWJ, Bolhuis H, Borin S, Daffonchio D, Corselli C, Giuliano L, et al. The enigma of prokaryotic life in deep hypersaline anoxic basins. Science. 2005;307:121–3.
13. Reed AJ, Lutz RA, Vetriani C. Vertical distribution and diversity of bacteria and archaea in sulfide and methane-rich cold seep sediments located at the base of the Florida escarpment. Extremophiles. 2006;10:199–211.
14. Campbell BJ, Engel AS, Porter ML, Takai K. The versatile ε-proteobacteria: Key players in sulphidic habitats. Nat Rev Microbiol. 2006;4:458–468.
15. Adam N, Perner M. Microbially mediated hydrogen cycling in deep-sea hydrothermal vents. Front Microbiol. 2018;9:1-17.
16. Ricci F, Greening C. Chemosynthesis: a neglected foundation of marine ecology and biogeochemistry. Trends Microbiol. 2024;32:631–639.
17. Campbell BJ, Jeanthon C, Kostka JE, Luther GW, Cary SC. Growth and Phylogenetic properties of novel bacteria belonging to the *Epsilon* subdivision of the *Proteobacteria* enriched from *Alvinella pompejana* and deep-sea hydrothermal vents. Appl Environ Microbiol. 2001;67:4566–72.
18. Nakagawa S, Takai K, Inagaki F, Hirayama H, Nunoura T, Horikoshi K, et al. Distribution, phylogenetic diversity and physiological characteristics of *epsilon-Proteobacteria* in a deep-sea hydrothermal field. Environ Microbiol. 2005;7:1619–32.
19. Smedile F, Foustoukos DI, Patwardhan S, Mullane K, Schlegel I, Adams MW, et al. Adaptations to high pressure of *Nautilia* sp. strain PV-1, a piezophilic *Campylobacterium* (aka *Epsilonproteobacterium*) isolated from a deep-sea hydrothermal vent. Environ Microbiol. 2022; 24:6164–83.
20. Wang L, Shen Z, Cheng X, Hwang JS, Guo Y, Sun M, et al. Metagenomic insights into the functions of microbial communities in sulfur-rich sediment of a shallow-water hydrothermal vent off Kueishan Island. Front Microbiol. 2022;13:992034.
21. Han Y, Perner M. The globally widespread genus *Sulfurimonas*: Versatile energy metabolisms and adaptations to redox clines. Front Microbiol. 2015;6:989.
22. Malik L, Hedrich S. Ferric Iron Reduction in Extreme Acidophiles. Front Microbiol. 2022;12:818414.
23. Sun QL, Xu K, Cao L, Du Z, Wang M, Sun L. Nitrogen and sulfur cycling driven by Campylobacterota in the sediment-water interface of deep-sea cold seep: A case in the South China Sea. mBio. 2023;14:e0011723.
24. Biderre-Petit C, Courtine D, Hennequin C, Galand PE, Bertilsson S, Debroas D, et al. A pan-genomic approach reveals novel *Sulfurimonas* clade in the ferruginous meromictic Lake Pavin. Mol Ecol Resour. 2024;24:e13923.
25. Molari M, Manini E, Dell'Anno A. Dark inorganic carbon fixation sustains the functioning of benthic deep-sea ecosystems. Global Biogeochem Cycles. 2013;27:212–21.
26. Ferrer M, Werner J, Chernikova TN, Bargiela R, Fernández L, La Cono V, et al. Unveiling microbial life in the new deep-sea hypersaline Lake Thetis. Part II: A metagenomic study. Environ Microbiol. 2012;14:268–81.
27. Assié A, Leisch N, Meier DV, Gruber-Vodicka H, Tegetmeyer HE, Meyerdierks A, et al. Horizontal acquisition of a patchwork Calvin cycle by symbiotic and free-living Campylobacterota (formerly *Epsilonproteobacteria*). ISME J. 2020;14:104–22.
28. Vetriani C, Voordeckers JW, Crespo-Medina M, O'Brien CE, Giovannelli D, Lutz RA. Deep-sea hydrothermal vent *Epsilonproteobacteria* encode a conserved and widespread nitrate reduction pathway (*Nap*). ISME J. 2014;8:1510–21.
29. Whaley-Martin KJ, Chen LX, Nelson TC, Gordon J, Kantor R, Twible LE, et al. O_2 partitioning of sulfur oxidizing bacteria drives acidity and thiosulfate distributions in mining waters. Nat Commun. 2023;14:2006.
30. Rossmassler K, Hanson TE, Campbell BJ. Diverse sulfur metabolisms from two subterranean sulfidic spring systems. FEMS Microbiol Lett. 2016;363:fhw162.
31. Patwardhan S, Foustoukos DI, Giovannelli D, Yücel M, Vetriani C. Ecological succession of sulfur-oxidizing *epsilon*- And *gammaproteobacteria* during colonization of a shallow-water gas vent. Front Microbiol. 2018;9:2970.
32. Pachiadaki MG, Yakimov MM, Lacono V, Leadbetter E, Edgcomb V. Unveiling microbial activities along the halocline of Thetis, a deep-sea hypersaline anoxic basin. ISME J. 2014;8:2478–89.
33. Rubin-Blum M, Makovsky Y, Rahav E, Belkin N, Antler G, Sisma-Ventura G, et al. Active microbial communities facilitate carbon turnover in brine pools found in the deep Southeastern Mediterranean Sea. Mar Environ Res. 2024; 198:106497.
34. Yakimov MM, La Cono V, Denaro R, D'Auria G, Decembrini F, Timmis KN, et al. Primary producing prokaryotic communities of brine,

interface and seawater above the halocline of deep anoxic lake L'Atalante. Eastern Mediterranean Sea ISME Journal. 2007;1:743–55.
35. Schmidt M, Al-Farawati R, Botz R. Geochemical classification of brine-filled Red Sea deeps. Berlin, Heidelberg: Springer; 2015. p. 219–33.
36. Ngugi DK, Blom J, Alam I, Rashid M, Ba-Alawi W, Zhang G, et al. Comparative genomics reveals adaptations of a halotolerant *Thaumarchaeon* in the interfaces of brine pools in the Red Sea. ISME J. 2015;9:396–411.
37. Hartmann M, Scholten JC, Stoffers P, Wehner F. Hydrographic structure of brine-filled deeps in the Red Sea-new results from the Shaban, Kebrit, Atlantis II, and Discovery Deep. Mar Geol. 1998;144:311–30.
38. Blum N, Puchelt H. Sedimentary-hosted polymetailic massive sulfide deposits of the Kebrit and Shaban Deeps. Red Sea Miner Depos. 1991;26:217–27.
39. Pautot G, Guennoc P, Coutelle A, Lyberis N. Discovery of a large brine deep in the northern Red Sea. Nature. 1984;310:133–6.
40. Michoud G, Ngugi DK, Barozzi A, Merlino G, Calleja ML, Delgado-Huertas A, et al. Fine-scale metabolic discontinuity in a stratified prokaryote microbiome of a Red Sea deep halocline. ISME J. 2021;15:2351–65.
41. Klindworth A, Pruesse E, Schweer T, Peplies J, Quast C, Horn M, et al. Evaluation of general 16S ribosomal RNA gene PCR primers for classical and next-generation sequencing-based diversity studies. Nucleic Acids Res. 2013;41:e1.
42. Callahan BJ, McMurdie PJ, Rosen MJ, Han AW, Johnson AJA, Holmes SP. DADA2: high-resolution sample inference from Illumina amplicon data. Nat Methods. 2016;13:581–3.
43. Bolyen E, Rideout JR, Dillon MR, Bokulich NA, Abnet CC, Al-Ghalith GA, et al. Reproducible, interactive, scalable and extensible microbiome data science using QIIME 2. Nat Biotechnol. 2019;37:852–7.
44. Quast C, Pruesse E, Yilmaz P, Gerken J, Schweer T, Yarza P, et al. The SILVA ribosomal RNA gene database project: Improved data processing and web-based tools. Nucleic Acids Res. 2013;41:D590-596.
45. Krueger F. Trim Galore: A wrapper around Cutadapt and FastQC to consistently apply adapter and quality trimming to FastQ files, with extra functionality for RRBS Data. Babraham Institute, United Kingdom, 2015
46. Andrews S. FastQC: A quality control tool for high throughput sequence data. Babraham Bioinformatics, Babraham Institute, Cambridge, United Kingdom. 2010; https://www.bioinformatics.babraham.ac.uk/projects/fastqc/
47. Martin M. Cutadapt removes adapter sequences from high-throughput sequencing reads. EMBnet J. 2011; https://journal.embnet.org/index.php/embnetjournal/article/view/200
48. Krueger F. Trim Galore. Babraham Bioinformatics, Babraham Institute, Cambridge, United Kingdom. 2018; https://www.bioinformatics.babraham.ac.uk/projects/trim_galore/
49. Li D, Liu CM, Luo R, Sadakane K, Lam TW. MEGAHIT: an ultra-fast single-node solution for large and complex metagenomics assembly via succinct de Bruijn graph. Bioinformatics. 2015;31:1674–6.
50. Nayfach S, Shi ZJ, Seshadri R, Pollard KS, Kyrpides NC. New insights from uncultivated genomes of the global human gut microbiome. Nature. 2019;568:505–10.
51. Uritskiy GV, Diruggiero J, Taylor J. MetaWRAP - A flexible pipeline for genome-resolved metagenomic data analysis. Microbiome. 2018;6:158.
52. Alneberg J, Bjarnason BS, De Bruijn I, Schirmer M, Quick J, Ijaz UZ, et al. Binning metagenomic contigs by coverage and composition. Nat Methods. 2014;11:1144–6.
53. Kang DD, Li F, Kirton E, Thomas A, Egan R, An H, et al. MetaBAT 2: An adaptive binning algorithm for robust and efficient genome reconstruction from metagenome assemblies. PeerJ. 2019;26:e7359.
54. Wu YW, Simmons BA, Singer SW. MaxBin 2.0: An automated binning algorithm to recover genomes from multiple metagenomic datasets. Bioinformatics. 2016;32:605–7.
55. Han P, Tang X, Koch H, Dong X, Hou L, Wang D, et al. Unveiling unique microbial nitrogen cycling and nitrification driver in coastal Antarctica. Nat Commun. 2024;15:3143.
56. Li Y, Chen J, Lin Y, Zhong C, Jing H, Liu H. *Thaumarchaeota* from deep-sea methane seeps provide novel insights into their evolutionary history and ecological implications. Microbiome. 2024;12:197.
57. Mikheenko A, Saveliev V, Gurevich A. MetaQUAST: evaluation of metagenome assemblies. Bioinformatics. 2016;32:1088–90.
58. Parks DH, Imelfort M, Skennerton CT, Hugenholtz P, Tyson GW. CheckM: assessing the quality of microbial genomes recovered from isolates, single cells, and metagenomes. Genome Res. 2015;25:1043–55.
59. Chklovski A, Parks DH, Woodcroft BJ, Tyson GW. CheckM2: a rapid, scalable and accurate tool for assessing microbial genome quality using machine learning. Nat Methods. 2023;20:1203–12.
60. Chaumeil PA, Mussig AJ, Hugenholtz P, Parks DH. GTDB-Tk: a toolkit to classify genomes with the genome taxonomy database. Bioinformatics. 2020;36:1925–7.
61. Parks DH, Chuvochina M, Rinke C, Mussig AJ, Chaumeil PA, Hugenholtz P. GTDB: an ongoing census of bacterial and archaeal diversity through a phylogenetically consistent, rank normalized and complete genome-based taxonomy. Nucleic Acids Res. 2022;50:785–94.
62. Olm MR, Brown CT, Brooks B, Banfield JF. DRep: a tool for fast and accurate genomic comparisons that enables improved genome recovery from metagenomes through de-replication. ISME J. 2017;11:2864–8.
63. Bushnell B. BBTools software package. 2014; sourceforge.net/projects/bbmap/
64. Oren A, Garrity GM. Valid publication of the names of forty-two phyla of prokaryotes. Int J Syst Evol Microbiol. 2021;71:005056.
65. Lee MD. GToTree: a user-friendly workflow for phylogenomics. Bioinformatics. 2019;35:4162–4.
66. Hug LA, Baker BJ, Anantharaman K, Brown CT, Probst AJ, Castelle CJ, et al. A new view of the tree of life. Nat Microbiol. 2016;1:16048.
67. Hyatt D, Chen G-L, Locascio PF, Land ML, Larimer FW, Hauser LJ. Prodigal: prokaryotic gene recognition and translation initiation site identification. 2010;11:119.
68. Potter SC, Luciani A, Eddy SR, Park Y, Lopez R, Finn RD. HMMER web server: 2018 update. Nucleic Acids Res. 2018;46:W200–4.
69. Price MN, Dehal PS, Arkin AP. FastTree 2 - approximately maximum-likelihood trees for large alignments. PLoS One. 2010;5:e9490.
70. Letunic I, Bork P. Interactive tree of life (iTOL) *v5*: an online tool for phylogenetic tree display and annotation. Nucleic Acids Res. 2021;49:W293–6.
71. Richter M, Rosselló-Móra R, Oliver Glöckner F, Peplies J. JSpeciesWS: a web server for prokaryotic species circumscription based on pairwise genome comparison. Bioinformatics. 2016;32:929–31.
72. Goris J, Konstantinidis KT, Klappenbach JA, Coenye T, Vandamme P, Tiedje JM. DNA-DNA hybridization values and their relationship to whole-genome sequence similarities. Int J Syst Evol Microbiol. 2007;57:81–91.
73. Qin QL, Xie B Bin, Zhang XY, Chen XL, Zhou BC, Zhou J, et al. A proposed genus boundary for the prokaryotes based on genomic insights. J Bacteriol. 2014; 196:2210–5.
74. Prokka ST. Rapid prokaryotic genome annotation. Bioinformatics. 2014;30:2068–9.
75. Kim D, Park S, Chun J. Introducing EzAAI: a pipeline for high throughput calculations of prokaryotic average amino acid identity. J Microbiol. 2021;59:476–80.
76. Wang S, Jiang L, Hu Q, Cui L, Zhu B, Fu X, et al. Characterization of *Sulfurimonas hydrogeniphila* sp. nov., a novel bacterium predominant in deep-sea hydrothermal vents and comparative genomic analyses of the genus *Sulfurimonas*. Front Microbiol. 2021;12:626705.
77. Moulana A, Anderson RE, Fortunato CS, Huber JA. Selection is a significant driver of gene gain and loss in the pangenome of the bacterial genus *Sulfurovum* in geographically distinct deep-sea hydrothermal vents. mSystems. 2020;5:1128.
78. Eren AM, Esen OC, Quince C, Vineis JH, Morrison HG, Sogin ML, et al. Anvi'o: An advanced analysis and visualization platformfor 'omics data. PeerJ. 2015;8:e1319.
79. Huerta-Cepas J, Szklarczyk D, Heller D, Hernández-Plaza A, Forslund SK, Cook H, et al. EggNOG 5.0: A hierarchical, functionally and phylogenetically annotated orthology resource based on 5090 organisms and 2502 viruses. Nucleic Acids Res. 2019;47:D309–14.
80. Zhou Z, Tran PQ, Breister AM, Liu Y, Kieft K, Cowley ES, et al. METABOLIC: high-throughput profiling of microbial genomes for functional traits, metabolism, biogeochemistry, and community-scale functional networks. Microbiome. 2022;10:33.
81. Rice P, Longden I, Bleasby A. EMBOSS: the European molecular biology open software suite. Trends Genet. 2000;16:276–7.

82. Quinn TP, Richardson MF, Lovell D, Crowley TM. propr: an R-package for identifying proportionally abundant features using compositional data analysis. Sci Rep. 2017;7:1–9.
83. Lovell D, Pawlowsky-Glahn V, Egozcue JJ, Marguerat S, Bähler J. Proportionality: a valid alternative to correlation for relative data. PLoS Comput Biol. 2015;11:e1004075.
84. Jameson BD, Murdock SA, Ji Q, Stevens CJ, Grundle DS, Kim JS. Network analysis of 16S rRNA sequences suggests microbial keystone taxa contribute to marine N_2O cycling. Communications Biology. 2023;6:212.
85. Bastian M, Heymann S, Jacomy M. Gephi : An Open Source Software for Exploring and Manipulating Networks Visualization and Exploration of Large Graphs. 2009; www.aaai.org.
86. Backer H, Schoell M. New deeps with brines and metalliferous sediments in the Red Sea. Nat Phys Sci. 1972;240:153–8.
87. Guan Y, Hikmawan T, Antunes A, Ngugi D, Stingl U. Diversity of methanogens and sulfate-reducing bacteria in the interfaces of five deep-sea anoxic brines of the Red Sea. Res Microbiol. 2015;166:688–99.
88. Eder W, Jahnke LL, Schmidt M, Huber R. Microbial diversity of the brine-seawater interface of the Kebrit Deep, Red Sea, studied via 16S rRNA gene sequences and cultivation methods. Appl Environ Microbiol. 2001;67:3077–85.
89. Jain C, Rodriguez-R LM, Phillippy AM, Konstantinidis KT, Aluru S. High throughput ANI analysis of 90K prokaryotic genomes reveals clear species boundaries. Nat Commun. 2018;9:5114.
90. Barco RA, Garrity GM, Scott JJ, Amend JP, Nealson KH, Emerson D. A genus definition for bacteria and archaea based on a standard genome relatedness index. mBio. 2020;11:10.1128.
91. Giovannoni SJ, Cameron Thrash J, Temperton B. Implications of streamlining theory for microbial ecology. ISME J. 2014;8:1553–65.
92. Borin S, Crotti E, Mapelli F, Tamagnini I, Corselli C, Daffonchio D. DNA is preserved and maintains transforming potential after contact with brines of the deep anoxic hypersaline lakes of the Eastern Mediterranean Sea. Saline Syst. 2008;4:10.
93. Salwan R, Sharma V. Genomics of prokaryotic extremophiles to unfold the mystery of survival in extreme environments. Microbiol Res. 2022;264:127156.
94. Lassalle F, Périan S, Bataillon T, Nesme X, Duret L, Daubin V. GC-content evolution in bacterial genomes: the biased gene conversion hypothesis expands. PLoS Genet. 2015;11:1–20.
95. Gunde-Cimerman N, Plemenitaš A, Oren A. Strategies of adaptation of microorganisms of the three domains of life to high salt concentrations. FEMS Microbiol Rev. 2018;42:353–75.
96. Oren A. Microbial life at high salt concentrations: Phylogenetic and metabolic diversity. Saline Syst. 2008;4:2.
97. Li R, Hou YN, Li H, Han Y, Zhang D, Song Y, et al. Salinity responsive mechanisms of sulfur-based mixotrophic denitrification and ectoine induced tolerance enhancement. Chem Eng J. 2024;496:154266.
98. Hügler M, Wirsen CO, Fuchs G, Taylor CD, Sievert SM. Evidence for autotrophic CO_2 fixation via the reductive tricarboxylic acid cycle by members of the ε subdivision of *proteobacteria*. J Bacteriol. 2005;187:3020–7.
99. Felden J, Ruff SE, Ertefai T, Inagaki F, Hinrichs KU, Wenzhöfer F. Anaerobic methanotrophic community of a 5346-m-deep vesicomyid clam colony in the Japan Trench. Geobiology. 2014;12:183–99.
100. Grünke S, Felden J, Lichtschlag A, Girnth AC, De Beer D, Wenzhöfer F, et al. Niche differentiation among mat-forming, sulfide-oxidizing bacteria at cold seeps of the Nile Deep Sea Fan (Eastern Mediterranean Sea). Geobiology. 2011;9:330–48.
101. Hughes NJ, Chalk PA, Clayton CL, Kelly DJ. Identification of carboxylation enzymes and characterization of a novel four-subunit pyruvate:flavodoxin oxidoreductase from *Helicobacter pylori*. J Bacteriol. 1995;177:3953–9.
102. Bayer B, Saito MA, McIlvin MR, Lücker S, Moran DM, Lankiewicz TS, et al. Metabolic versatility of the nitrite-oxidizing bacterium *Nitrospira marina* and its proteomic response to oxygen-limited conditions. ISME J. 2021;15:1025–39.
103. Fuchs G. Alternative pathways of carbon dioxide fixation: Insights into the early evolution of life? Annu Rev Microbiol. 2011;65:631–58.
104. Castaño-Cerezo S, Pastor JM, Renilla S, Bernal V, Iborra JL, Cánovas M. An insight into the role of phosphotransacetylase (pta) and the acetate/acetyl-CoA node in *Escherichia coli*. Microb Cell Fact. 2009;8:54.
105. Wood AP, Aurikko JP, Kelly DP. A challenge for 21st century molecular biology and biochemistry: What are the causes of obligate autotrophy and methanotrophy? FEMS Microbiol Rev. 2004;28:335–352.
106. Winkel M, Pjevac P, Kleiner M, Littmann S, Meyerdierks A, Amann R, et al. Identification and activity of acetate-assimilating bacteria in diffuse fluids venting from two deep-sea hydrothermal systems. FEMS Microbiol Ecol. 2014;90:731–46.
107. Kaartvedt S, Antunes A, Røstad A, Klevjer TA, Vestheim H. Zooplankton at deep Red Sea brine pools. J Plankton Res. 2016;38:679–84.
108. Sudo M, Osvatic J, Taylor JD, Dufour SC, Prathep A, Wilkins LGE, et al. *SoxY* gene family expansion underpins adaptation to diverse hosts and environments in symbiotic sulfide oxidizers. mSystems. 2024;9:e01135-23.
109. Akerman NH, Butterfield DA, Huber JA. Phylogenetic diversity and functional gene patterns of sulfur-oxidizing subseafloor *Epsilonproteobacteria* in diffuse hydrothermal vent fluids. Front Microbiol. 2013;4:185.
110. Wang Z, Wang S, Lai Q, Wei S, Jiang L, Shao Z. *Sulfurimonas marina* sp. nov., an obligately chemolithoautotrophic, sulphur-oxidizing bacterium isolated from a deep-sea sediment sample from the South China Sea. Int J Syst Evol Microbiol. 2022;72:005582.
111. Li J, Törkel K, Koch J, Tanabe TS, Hsu HY, Dahl C. In the Alphaproteobacterium *Hyphomicrobium denitrificans SoxR* serves a sulfane sulfur-responsive repressor of sulfur oxidation. Antioxidants. 2023;12:1620.
112. Ghosh W, Dam B. Biochemistry and molecular biology of lithotrophic sulfur oxidation by taxonomically and ecologically diverse bacteria and archaea. FEMS Microbiol Rev. 2009;33:999–1043.
113. Gwak J-H, Awala SI, Nguyen N-L, Yu W-J, Yang H-Y, Von Bergen M, et al. Sulfur and methane oxidation by a single microorganism. PNAS. 2022;119:e2114799119.
114. Tanaka Y, Yoshikaie K, Takeuchi A, Ichikawa M, Mori T, Uchino S, et al. Crystal structure of a YeeE/YedE family protein engaged in thiosulfate uptake. Science Advance. 2020;6:eaba7637.
115. Vignais PM, Colbeau A. Molecular biology of microbial hydrogenases. Curr Issues Mol Biol. 2004;6:159–88.
116. Han Y, Perner M. The role of hydrogen for *Sulfurimonas denitrificans* metabolism. PLoS One. 2014;9:e106218.
117. Mwirichia R, Alam I, Rashid M, Vinu M, Ba-Alawi W, Anthony Kamau A, et al. Metabolic traits of an uncultured archaeal lineage-MSBL1-from brine pools of the Red Sea. Sci Rep. 2016;6:19181.
118. Pitcher RS, Brittain T, Watmoug NJ. Cytochrome *cbb3* oxidase and bacterial microaerobic metabolism. Biochem Soc Trans. 2002;30:653–8.
119. Johnson LA, Hug LA. Distribution of reactive oxygen species defense mechanisms across domain bacteria. Free Radic Biol Med. 2019;140:93–102.
120. Pitcher RS, Watmough NJ. The bacterial cytochrome cbb3 oxidases. Biochim Biophys Acta. 2004;1655:388–99.
121. Kendall JJ, Barrero-Tobon AM, Hendrixson DR, Kelly DJ. Hemerythrins in the microaerophilic bacterium *Campylobacter jejuni* help protect key iron-sulphur cluster enzymes from oxidative damage. Environ Microbiol. 2014;16:1105–21.
122. French CE, Bell JML, Ward FB. Diversity and distribution of hemerythrin-like proteins in prokaryotes. FEMS Microbiol Lett. 2008;279:131–45.
123. Troxell B, Hassan HM. Transcriptional regulation by ferric uptake regulator (Fur) in pathogenic bacteria. Front Cell Infect Microbiol. 2013;3:59.
124. Fontenot CR, Tasnim H, Valdes KA, Popescu CV, Ding H. Ferric uptake regulator (Fur) reversibly binds a [2Fe-2S] cluster to sense intracellular iron homeostasis in *Escherichia coli*. J Biol Chem. 2020;295:15454–63.
125. Lau CKY, Krewulak KD, Vogel HJ. Bacterial ferrous iron transport: the Feo system. FEMS Microbiol Rev. 2016;40:273–98.
126. Spiro S, Guest JR. FNR and its role in oxygen-regulated gene expression in *Escherichia coli*. FEMS Microbiol Lett. 1990;75:399–428.
127. Kammler M, Schon C, Hantke K. Characterization of the ferrous iron uptake system of *Escherichia coli*. J Bacteriol. 1993;175:6212–9.
128. Oren A. Thermodynamic limits to microbial life at high salt concentrations. Environ Microbiol. 2011;13:1908–23.

Publisher's Note